Interaction Between Alkali Chlorides and Ilmenite in Chemical Looping Combustion

N.B. When citing this work, cite the original published paper.

(article starts on next page)

Article

Interaction Between Alkali Chlorides and Ilmenite in Chemical Looping Combustion

Published as part of Energy & Fuels special issue "2024 Pioneers in Energy Research: Juan Adanez".

Ashwani Kumar Dubey,* Daofeng Mei, Anders Lyngfelt, Tobias Mattisson, and Henrik Leion

Read Online

ACCESS | Metrics & More | Article Recommendations

ABSTRACT: Chemical looping combustion (CLC) is an emerging combustion technology recognized for its high efficiency and minimal environmental impact in terms of CO_2 emissions. When biomass is used in CLC, the process referred to as Bio-CLC, it can result in negative CO_2 emissions. However, the presence of alkalis (K and Na) in biomass can pose operational challenges. To better understand how alkalis interact with oxygen carriers, this study utilized a method involving the impregnation of charcoal particles with alkali salts (KCl or NaCl or both). The influence of alkali chlorides on fluidization/agglomeration, reactivity, and interaction with ilmenite was investigated in a batch fluidized bed reactor operating at 950 °C. During the reduction step of the simulated CLC cycles with solid fuels, charcoal impregnated with KCl (K-charcoal), NaCl (Na-charcoal), and a combination of both (Na−K charcoal) was used. A total of 33 alkali cycles were performed with K-charcoal, Na-charcoal, and Na−K charcoal with calcined ilmenite, as well as Na−K charcoal with synthetic ilmenite, including additional cycles using nonimpregnated charcoal as a reference. Na−K charcoal with calcined ilmenite led to an earlier onset of agglomeration and defluidization than single-impregnated charcoal. In contrast, no defluidization was observed in the case of synthetic ilmenite with Na−K charcoal. EDX analyses revealed minimal Na and no K accumulation in the particle bridges of the final Na-ilmenite and K-ilmenite samples. Conversely, Na and K were found together with Si and Al in the particle bridges of the final Na−K ilmenite, while no accumulation of Na and K was observed in the final Na−K synthetic ilmenite. ICP-OES analyses showed that approximately 28% of K and 49% of Na were retained in the final K-ilmenite and Na-ilmenite, respectively. Negative K retention and 40% Na were observed in the final Na−K ilmenite, whereas 35% K and 40% Na retention were found in the final Na−K synthetic ilmenite. This research significantly enhances our understanding of the interactions between alkali chlorides and ilmenite.
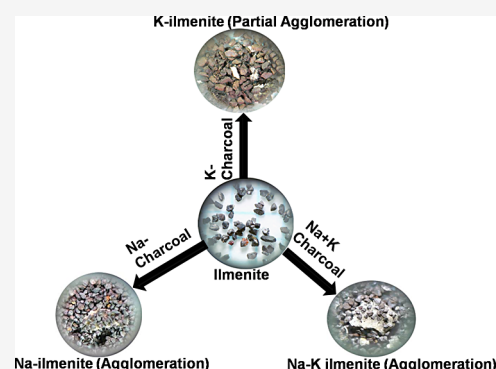
1. INTRODUCTION

The combustion of fossil fuels provides energy and power worldwide, and the carbon dioxide (CO_2) emitted into the atmosphere from the combustion of fossil fuels is the main contributor to global warming and climate change. According to the Sixth Assessment Report by the Intergovernmental Panel on Climate Change (IPCC), the Earth's surface average temperature was 1.1 °C higher from 2011 to 2020 compared to the period from 1850 to 1900.[1] This global concern has driven extensive research into developing cost-effective methods for capturing CO_2. Three potential approaches for capturing CO_2 from fossil fuels power plants have been examined: precombustion, postcombustion, and oxy-fuel combustion.[2,3] Chemical looping combustion (CLC) has received significant attention due to its ability to integrate fossil fuel combustion with inherent CO_2 capture, offering high thermoeconomic efficiency at low cost.[4−6] Unlike oxy-fuel combustion techniques, CLC does not require pure oxygen. Instead, it utilizes a suitable metal oxide as an oxygen carrier to transfer oxygen to the fuel reactor. Transitioning from fossil fuels to biomass, which is considered renewable and CO_2-neutral, offers a potential method for reducing CO_2 emissions. Furthermore, when biomass is used in combustion systems equipped with carbon capture and storage (CCS), negative CO_2 emissions can be achieved. Thus, CLC can contribute to negative CO_2 emissions when used for bioenergy carbon capture and storage (BECCS).[7−9]
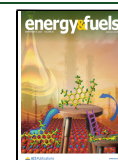
The basic principle of CLC involves the circulation of oxygen carriers between two reactors: a fuel reactor (FR) and an air reactor (AR), as illustrated in Figure 1. In the FR, the
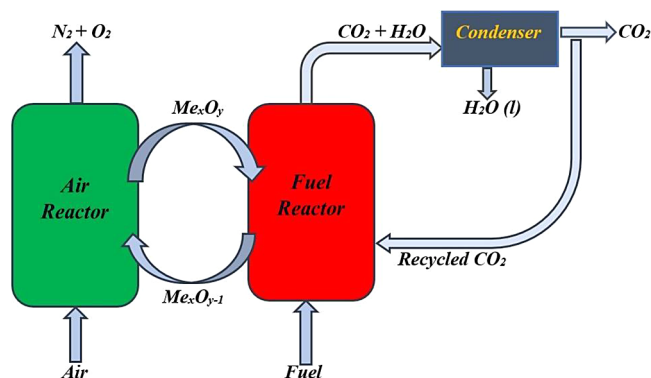
Figure 1. Schematic description of the chemical looping combustion process.

oxygen carrier reacts with the fuel, enabling the combustion process.[6−9] The resulting gaseous products, ideally only steam and CO_2, are easily separated, allowing for CO_2 and subsequent storage or utilization. The oxygen carrier, having lost some oxygen, is then transported to the AR, where it undergoes regeneration. In the AR, the oxygen carrier is exposed to an oxygen-rich environment (i.e., air), allowing it to replenish its oxygen content. The regenerated oxygen carrier is then returned to the FR to initiate another combustion cycle.

The key advantages of CLC include the inherent production of a concentrated CO_2 stream and simplification of the capture and storage compared to conventional combustion processes. By separating the fuel and air streams, CLC avoids the exergy losses associated with CO_2 dilution in nitrogen and the high energy and cost penalties of other CO_2 capture technologies, resulting in a higher overall system efficiency.

CLC is versatile and adaptable to various energy sources, as it can be applied to a wide range of fuels, including solid, liquid, and gaseous fuels.[4] Additionally, CLC can reduce or eliminate the formation of nitrogen oxides (NO_x) and other harmful pollutants.[10] It can also be integrated with other energy conversion processes, such as gasification[11,12] or steam-methane reforming.[13] Designs for full-scale CLC boilers have been proposed by Lyngfelt et al.[14,15] and Abad et al.[16]

Ilmenite, a natural iron−titanium oxide mineral ($FeTiO_3$), has gained significant attention as an oxygen carrier material in CLC due to its unique properties and advantages.[4,17,18] Ilmenite is a widely available mineral that is found in large quantities worldwide, making it is a cost-effective and sustainable choice for large-scale CLC applications. Ilmenite demonstrates favorable redox properties, which means it can easily undergo oxidation and reduction reactions. This characteristic is crucial for the cyclic operation of CLC, where the oxygen carrier alternates between the oxidized and reduced states. Additionally, Ilmenite exhibited good chemical stability under the CLC operating conditions.[19,20] Overall, ilmenite offers several advantages as an oxygen carrier in CLC, making it a promising material for advancing clean and efficient energy-conversion technologies.

In the CLC process, ash represents the noncombustible residue that remains in the FR after combustion. For large-scale CLC systems, effective removal of ash is crucial to prevent accumulation and potential operational complications.[4−9] This issue is particularly significant in biomass-based CLC due to high levels of alkali metals (such as Na and K) in biomass compared to coal.[21] Alkali metals play a significant role during biomass gasification by catalyzing char gasification, thus accelerating biomass conversion.[22−25] These alkali metals

Table 1. Summary of the Experimental Studies of the Interaction Between Different Alkalis with Ilmenite

sr. no.	alkali salts	bed material	fluidizing gas/fuel	reactor type	operational temperature	reference
1	K_2CO_3 and Na_2CO_3	Ilmenite	CO and CO_2	quartz batch fluidized bed reactor	900 °C	26
2	KCl, K_2SO_4, K_2CO_3	Quartz Sand	H_2O, dry air	fluidized bed reactor	750, 800, 850, 950 °C	27
3	K_2CO_3, K_2SO_4, KCl, KH_2PO_4	Ilmenite, Sand	air, steam	fluidized bed reactor	850, 950 °C	28
4	K_2CO_3	Ilmenite and Calcium Manganite perovskite	Black Pellets, Black Pellets impregnated with K_2CO_3, Straw Pellets, Wood Char	100 kW Chemical looping pilot plant	931−970 °C	29
5	K_2CO_3, K_2SO_4, KCl, KH_2PO_4	Ilmenite	CO and steam, H_2 and steam	fixed bed reactor, TGA	850 °C	30
6	Potassium salts	Ilmenite and Braunite	wood pellets, wood char, straw pellets	60 kWth Dual circulating fluidized bed	>800 °C	31
7	K and Na in fuel	Ilmenite	wood pellets, Swedish wood char, German wood char, pine forest residue, straw pellets	10 kWth Chemical looping pilot plant	885−988 °C	32
8	Na and K in fuel	Ilmenite and Braunite	wood pellets, wood char, Straw pellets	60 kWth a Dual circulating fluidized bed	793−857 °C	33
9	Sodium Phytate	Ilmenite	Nitrogen, Air, CO, CO_2	fixed bed reactor, Quartz batch fluidized bed reactor	1100, 850 °C	34
10	Na and K alkali	Ilmenite	Nitrogen, Synthetic gas	TGA	up to 1000 °C	35
11	K_2CO_3, KH_2PO, K_2SO_4	Ilmenite, Iron sand, LD slag, Mill scale	2.5% H_2 and 10% steam in Ar and N_2	horizontal fixed bed reactor	900 °C	36
12	K_2CO_3	Ilmenite	Methane, Syngas	steel batch fluidized bed reactor	850, 950 °C	37
13	K_2CO_3, KOH	Ilmenite	N_2, Air, CO_2, 6% CO in N_2	batch fluidized bed reactor	700, 800, 850, 900 °C	38
14	K_2CO_3, K_2SO_4, KH_2PO_4	Ilmenite, LD slag	H_2/steam, N_2/steam, Ar/H_2	horizontal fixed bed reactor	900 °C	39

Table 2. Composition of Charcoal, K-Charcoal, Na-Charcoal, Na−K Charcoal

	proximate analysis (wt %)				ultimate analysis (wt %)				metals (wt %)				
	FC	VM	M	A	C	H	N	S	Al	Si	Ca	K	Na
charcoal	84.3	4.9	1.9	8.9	89	<0.3	0.5	0.7	1.0	2.7	0.1	0.05	0.03
K-charcoal	55.7	6.4	8.9	29.0	64	<0.5	0.3	0.5	0.6	1.6	0.1	5.2	0.04
Na-charcoal	62.7	5.5	6.8	25.0	71	<0.5	0.4	0.3	0.8	2.0	0.1	0.03	5.2
Na−K charcoal	67.4	6.4	1.2	25.3	62	1.9	0.3	0.4	0.8	2.0	0.1	5.1	3.8

Table 3. Chemical Composition of Calcined Ilmenite, Synthetic Ilmenite, and Calcined Ilmenite Samples Used with K-charcoal, Na-charcoal, Na−K charcoal, and Synthetic Ilmenite Used with Na−K Charcoal Determined by the ICP-SFMS Technique (Weight %, Dry Basis[a])

	Fe	Ti	Mg	Si	Al	Mn	Ca	K	Na
calcined ilmenite	33.50	22.20	2.20	1.86	0.29	0.18	0.34	0.31	0.05
synthetic ilmenite	38.70	15.20	<0.01	0.61	0.05	0.03	<0.05	<0.02	<0.02
K-ilmenite middle	39.60	24.60	1.45	1.25	0.45	0.19	0.20	0.64	0.06
Na-ilmenite middle	36.10	22.10	2.43	2.96	0.44	0.19	0.40	0.26	0.40
Na−K ilmenite middle	34.20	21.00	1.42	1.99	0.28	0.20	0.14	0.14	0.19
Na−K synthetic ilmenite middle	40.10	28.90	0.01	1.08	0.15	0.28	0.05	0.25	0.22
K-ilmenite	35.10	22.30	1.70	0.91	0.36	0.19	0.15	0.55	0.04
Na-ilmenite	34.80	22.60	2.43	2.83	0.43	0.19	0.34	0.21	0.47
Na−K ilmenite	37.70	23.90	1.53	2.10	0.36	0.23	0.15	0.22	0.30
Na−K synthetic ilmenite	38.20	26.90	0.02	1.53	0.21	0.04	0.07	0.31	0.27

[a]Calcined ilmenite refers to an ilmenite that has been calcined before any experiments. The terms K-ilmenite middle, Na-ilmenite middle, and Na−K ilmenite middle refer to samples taken after the middle cycles of oxidation−reduction experiments with the respective alkali charcoal samples. Similarly, K-ilmenite, Na-ilmenite, and Na−K ilmenite refer to samples taken after 33 oxidation−reduction cycles with the respective alkali charcoal samples. Synthetic ilmenite refers to synthetic ilmenite before any experiments. Na−K synthetic ilmenite middle refers to synthetic ilmenite samples taken after the middle cycle, and Na−K synthetic ilmenite refers to synthetic ilmenite samples taken after 33 oxidation−reduction cycles with Na−K charcoal (cf. Table 4 below).

can interact with oxygen carriers and other components of the CLC system, leading to various effects and operational challenges. They can react with other components in the fuel ash to form low-melting-point compounds, which can result in the agglomeration of bed material and fouling and corrosion of heat transfer surfaces downstream of the FR. Such deposits can hinder gas−solid interactions, reduce heat transfer efficiency, and cause operational problems. This can result in increased maintenance requirements, reduced system life spans, and increased operational costs. Additionally, the presence of alkali metals can introduce system instability and performance fluctuations during CLC operation. Their interaction with oxygen carriers can cause inconsistent and unpredictable reactivity, affecting oxygen transfer efficiency and overall combustion performance. This can result in reduced system reliability and difficulty maintaining stable operating conditions. Table 1 provides a brief review of research activities on different alkalis with ilmenite. The issues associated with alkalis are well-documented from conventional combustion processes, such as in fluidized beds.[21−23]

This research emphasizes alkali chlorides over alkali carbonates in the context of CLC, primarily due to their distinct chemical behaviors and associated operational impacts. Alkali chlorides are notably corrosive, especially under the elevated temperatures typical of the CLC process. They tend to generate volatile and corrosive compounds, such as HCl,[30] which pose significant challenges by accelerating the degradation of reactor materials, including oxygen carriers and structural components. This corrosion necessitates frequent maintenance interventions, thereby escalating operational costs and increasing the risk of downtime due to material failures. In contrast, while alkali carbonates can induce some corrosion, their effects are generally less severe compared to those of chlorides. Alkali carbonates exhibit a lower propensity to form volatile and highly corrosive compounds, thus presenting a comparatively lower risk to reactor integrity and operational reliability in CLC systems.

The interaction between ilmenite and alkali chlorides presents a multifaceted research domain encompassing a fundamental understanding, practical implications, and optimization possibilities. Alkali chlorides, such as sodium chloride (NaCl) and potassium chloride (KCl), can influence the reactivity of ilmenite by catalyzing. Additionally, the potential for alkali chloride deposition on the surfaces of ilmenite particles introduces challenges related to agglomeration, fouling, and particle attrition within the reactor system. Balancing the advantages of ilmenite's high oxygen-carrying capacity with the potential drawbacks associated with alkali-chloride interactions is pivotal for achieving efficient and robust CLC processes. In this context, this study systematically explores the interaction between ilmenite and alkali chlorides (KCl and NaCl) through both experimental investigations and theoretical analyses. It aims to understand the effects of alkali chlorides on the reactivity of ilmenite, its propensity to agglomerate, and other significant physical and chemical characteristics. Charcoal particles impregnated with alkali salts (KCl and/or NaCl) were used as fuel in a batch fluidized bed reactor during the reduction reaction. To investigate the agglomeration and defluidization caused by the interaction between alkali chlorides and ilmenite, 33 oxidation−reduction cycles were conducted with each alkali fuel and natural calcined ilmenite. For comparison, cycles using charcoal without alkali impregnation and methane were also performed. Additionally, 33 oxidation−reduction cycles were carried out

using synthetic ilmenite with Na−K charcoal. These results were compared with those obtained from natural calcined ilmenite cycles using Na−K charcoal. This study highlights the interaction between alkali (Na and K) and ilmenite, as well as the role of silica (SiO_2) in the agglomeration. After the final cycles, the reactivity of the bed material, composition, and microstructure were thoroughly evaluated using various characterization techniques.

2. EXPERIMENTAL SECTION

2.1. Fuels and Oxygen Carrier. In the CLC process, the main fuel elements present in the gas phase are CH_4, CO, and H_2. Therefore, reactivity analysis of fresh and used ilmenite was carried out using CH_4 and syngas (50% CO + 50% H_2) in a batch fluidized bed reactor, as outlined in Section 2.3. Charcoal and charcoal impregnated with KCl, NaCl, or a combination of both (KCl and NaCl) were employed as solid fuels, and the impregnated charcoals were denoted as K-charcoal, Na-charcoal, and Na−K charcoal, respectively. Charcoal with a porosity of approximately 0.47 mL/g was produced by pyrolysis of bituminous coal.[25] The charcoal was subsequently crushed and sieved to obtain particles with sizes ranging from 1 to 1.25 mm.

The preparation of K-charcoal, Na-charcoal, and Na−K charcoal involved an incipient dry impregnation method, detailed in a previous study.[25] In this method, a known concentration of the alkali solution is gradually introduced while stirring. The impregnated charcoal was then placed on a heated plate set to approximately 150 ± 10 °C, allowing for gradual drying to eliminate water and obtain the alkali-impregnated charcoal. Prior to alkali impregnation, the initial charcoal was comprised of 84.3% fixed carbon, 4.9% volatile matter, 8.9% ash, and 1.9% moisture, with minimal alkali content. Following impregnation, K-charcoal contained 5.2% K, Na-charcoal contained 5.2% Na, and Na−K charcoal contained 5.1% K and 3.8% Na. Silicon was observed in all four charcoal samples as indicated in Table 2.

In this study, both natural ilmenite and synthetic ilmenite were utilized as oxygen carriers. Before the experiments, natural ilmenite was calcined at 950 °C for 12 h to enhance particle strength and subsequently sieved to achieve a size range of 0.1−0.3 mm. Conversely, synthetic ilmenite was fabricated via freeze granulation and sintered at 1100 °C. The synthetic ilmenite, comprising 50% Fe_2O_3 and 50% TiO_2 by weight, transformed into pseudobrookite (Fe_2TiO_5) during the sintering process. The particle size of the synthetic ilmenite ranged from 0.1 to 0.3 mm. The elemental compositions of both calcined and synthetic ilmenite are detailed in Table 3.

2.2. Lab-Scale Batch Fluidized Bed Reactor Setup. Oxidation and reduction cycles were carried out by subjecting the oxygen carrier alternately to fuel and an oxidizing environment in a batch-fluidized bed setup,[40,41] as depicted in Figure 2. The apparatus consisted of a vertical quartz glass reactor with an internal diameter of 22 mm and a height of 820 mm. A porous quartz plate supporting the bed material was positioned 370 mm from the bottom. The reactor was encircled by an electrically heated furnace and its inlet and outlet were sealed to

prevent gas leakage. The reactor temperature was monitored using a K-type thermocouple placed within the bed. The reactive gas environment in the reactor tube was regulated using three magnetic valves, enabling settings for oxidation, inert, and reduction states, denoted as "Ox," "Inert," and "Red" in Figure 2. When one of the three channels was open, the remaining two channels were automatically closed. Cycling between oxidation, inert, and reduction modes was automated through a computer program, which alternated between "Ox," "Inert," and "Red." For the reduction reaction, gaseous fuels (methane or syngas) were introduced from the lower section of the reactor, while solid fuel was injected from the upper portion using a continuous stream of N_2 gas for sweeping. To prevent gas condensation, a heating band was set up in the upper section of the reactor to maintain the elevated temperatures. The pressure difference over the bed was monitored using a transducer connected to the top and bottom of the reactor to track fluidization conditions.[42,43] Following steam condensation in the downstream cooler, the outgoing gas was directed to a gas analyzer (NGA 2000, Rosemount) to assess CH_4, CO, CO_2, H_2, and O_2 concentrations. Parameters such as temperature, gas composition, volumetric flow, and pressure drop were consistently recorded using a computer connected to a data-logging system.

2.3. Experimental Procedure in Batch Fluidized Bed Reactor. *2.3.1. Four Series of Alkali Experiments.* At the start of the experiments, 20 g of ilmenite particles was placed on the porous quartz plate. The furnace was gradually heated to 950 °C under an inert atmosphere. Reduction and oxidation in the CLC were simulated by alternately subjecting the oxygen carrier to fuel (methane, syngas, charcoal, K-charcoal, Na-charcoal, and Na−K charcoal) and to an oxidizing environment (5% O_2 and 95% N_2). An inert atmosphere was maintained for 180 s between the oxidation and reduction periods by the injection of nitrogen to avoid gas mixing. During the reduction phase employing gaseous fuels, either methane or syngas was utilized. The inlet to the reactor maintained a constant normalized fuel flow rate of 345 mL/min for methane and 450 mL/min for syngas. For the solid fuel experiments, the gasification or fluidization gas contained a mixture of 48% H_2O and 52% N_2 with a total normalized flow rate of 750 mL/min. During the reduction period with solid fuels, approximately 0.1 g of solid fuel (charcoal, K-charcoal, Na-charcoal, or Na−K charcoal) was introduced from the top of the reactor using N_2 with a flow rate of 300 mL/min as sweep gas. A total of 33 redox cycles were performed using different alkali fuels, and Table 4 lists the alkali experiments. Across all experimental series, the oxygen carrier underwent an initial stabilization period involving methane cycles before using solid fuel. Three cycles were conducted using charcoal without alkali as the reference. Subsequently, the oxygen carrier was subjected to a series of cycles using alkali fuel. Alternating rounds of charcoal and alkali fuel were used. Samples of solid material were taken from the middle cycles, marked as "K-ilmenite middle," etc., for different types of fuel. Similarly, samples from the final cycles were labeled as "K-ilmenite," etc. The reactivities of calcined ilmenite and used ilmenite with syngas were investigated.

2.3.2. Reactivity of Ilmenite with Methane and Syngas. In each series of experiments, ilmenite underwent an initial activation phase involving methane cycling before the introduction of solid fuel. The reactivity of methane with ilmenite subjected to cycles with K-charcoal, Na-charcoal, and Na−K charcoal was compared to its reactivity in the initial cycle prior to charcoal addition. This comparison aimed to investigate the effects of K-charcoal, Na-charcoal, and Na−K charcoal on ilmenite reactivity.

To evaluate the reactivity of ilmenite samples with syngas, a separate series of experiments were conducted at 950 °C using calcined ilmenite, synthetic ilmenite, K-ilmenite final, Na-ilmenite final, Na−K ilmenite final, and Na−K synthetic ilmenite final samples. In these experiments, 2 g of used ilmenite was mixed with 13 g of sand. These mixtures underwent reaction cycles with a syngas flow rate of 450 mL/min, maintaining a gas velocity of 0.4 m/s at 950 °C. To ensure incomplete conversion of CO and H_2 in the syngas, ilmenite was diluted with sand, allowing for detailed data evaluation as
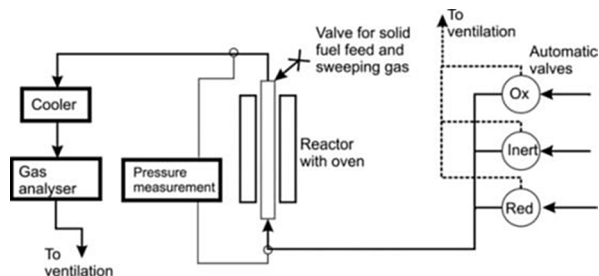

Figure 2. Schematic description of the batch fluidized bed reactor system.

Table 4. Experimental Series of K-Charcoal, Na-Charcoal, and Na−K Charcoal with CH₄ (■), Charcoal (■), and Alkali Fuels (■); Bold "M" Indicates the Middle Cycle for Bed Material Sampling; Syngas Cycles are not Shown Here

Alkali Series	Cycle number																			
Cycle 1-20	1	2	3	4	5	6	7	8	9	10	11	12	13	14	15	16	17	18	19	20
K-charcoal series with calcined ilmenite																				
Na-charcoal series with calcined ilmenite																				
Na-K charcoal series with calcined ilmenite																				
Na-K charcoal series with synthetic ilmenite																				
Cycle 21-40	21	22	23	24	25	26	27	28	29	30	31	32	33	34	35	36	37	38	39	40
K-charcoal series with calcined ilmenite																			**M**	
Na-charcoal series with calcined ilmenite																				**M**
Na-K charcoal series with calcined ilmenite											**M**									
Na-K charcoal series with synthetic ilmenite																				
Cycle 41-60	41	42	43	44	45	46	47	48	49	50	51	52	53	54	55	56	57	58	59	60
K-charcoal series with calcined ilmenite																				
Na-charcoal series with calcined ilmenite																				
Na-K charcoal series with calcined ilmenite																				
Na-K charcoal series with synthetic ilmenite				**M**																

outlined in Section 3 of the study. The experimental setup involved 10 cycles for the calcined ilmenite and 8 cycles for the synthetic ilmenite samples. In contrast, the K-ilmenite final, Na-ilmenite final, Na−K ilmenite final, and Na−K synthetic ilmenite final samples were subjected to 13, 13, 10, and 10 cycles, respectively.

2.4. Characterization Techniques. Proximate analysis (moisture, ash, and volatile matter) of the solid fuels (Charcoal, K-charcoal, Na-charcoal, and Na−K charcoal) was conducted using a Leco TGA-701 analyzer, while ultimate analysis (carbon, hydrogen, nitrogen, and sulfur) was performed using a Leco CHN-628 analyzer. These analyses were carried out according to various methods specified by the International Organization of Standardization (ISO) standards.[44−49] Scanning electron microscopy (SEM) combined with energy-dispersive X-ray spectroscopy (EDX) was employed to observe the physical and chemical changes in the ilmenite samples. These ilmenite samples were embedded in epoxy resin and polished to expose a cross-section of the particles for analysis. SEM (JEOL JSM-7800F Prime) was used to examine the microstructure and EDX (Oxford X-Max) was used for chemical analysis. The crystal phase compositions of the ilmenite samples were investigated using X-ray diffraction (XRD) with a Bruker D8 Advance. Ilmenite samples were ground, placed on the sample holder, and pressed vertically with a glass plate to ensure a flat surface. XRD scanning was conducted from 10 to 90° in steps of 0.3°/s, utilizing CuKα radiation at 40 mA and 40 kV. The structure of the oxygen carrier samples was observed under a light microscope (MICRO-80150, TAGARNO). Metal elements in the solid fuel and oxygen carrier particles were quantified using Inductively coupled plasma-sector field mass spectrometry (ICP-SFMS) with Thermo Scientific Element ICP-MS version 3.1.2.242, following a modified ASTM D3682 procedure.[50]

3. DATA EVALUATION

3.1. Gaseous Fuels. The concentration of the gases obtained from the experiments was used to evaluate fuel conversion. The parameters used to quantify this conversion included the mass-based conversion (ω) of the oxygen carrier and the yields (γ) of methane and syngas. The mass-based conversion (ω) of the oxygen carrier indicates the degree of reduction in the oxygen carrier during the reduction phase. This reduction corresponds to the amount of oxygen carrier consumed by the fuel. The mass-based conversion of the oxygen carrier was calculated using eq 1, where $\omega = 1$ signifies a fully oxidized state of the oxygen carrier. In this equation, m represents the actual mass of the oxygen carrier, m_{ox} represents the mass of the oxygen carrier in its fully oxidized state, and Δm signifies the mass loss of the oxygen carrier consumed by the fuel.

$$\omega = \frac{m}{m_{ox}} = \frac{m_{ox} - \Delta m}{m_{ox}} = 1 - \frac{\Delta m}{m_{ox}} \tag{1}$$

The mass-based conversion of the oxygen carrier for methane (ω_{CH_4}) and syngas (ω_{syn}) can be calculated using the following equations, eqs 2 and 3, respectively. These equations utilize the concentrations of various gases obtained from the gas analyzer.

$$\omega_{CH_4} = 1 - \int_{t_0}^{t} \frac{\dot{n}_{out} M_O}{m_{ox}} (4 x_{co_2} + 3 x_{co} - x_{H_2}) dt \tag{2}$$

$$\omega_{syn} = 1 - \int_{t_0}^{t} \frac{\dot{n}_{out} M_O}{m_{ox}} (2 x_{co_2} + x_{co} - x_{H_2}) dt \tag{3}$$

Here, $\dot{n}_{out}$ represents the molar flow rate of dry gas at the reactor exit, determined by calibrating the flow readings from the gas analyzer.[41] M_O stands for the molar mass of oxygen, and x_{co_2}, x_{co}, and x_{H_2} denote the instantaneous concentration of CO_2, CO, and H_2 at time t. t_0 and t represent the initial and final times of measurement, respectively.
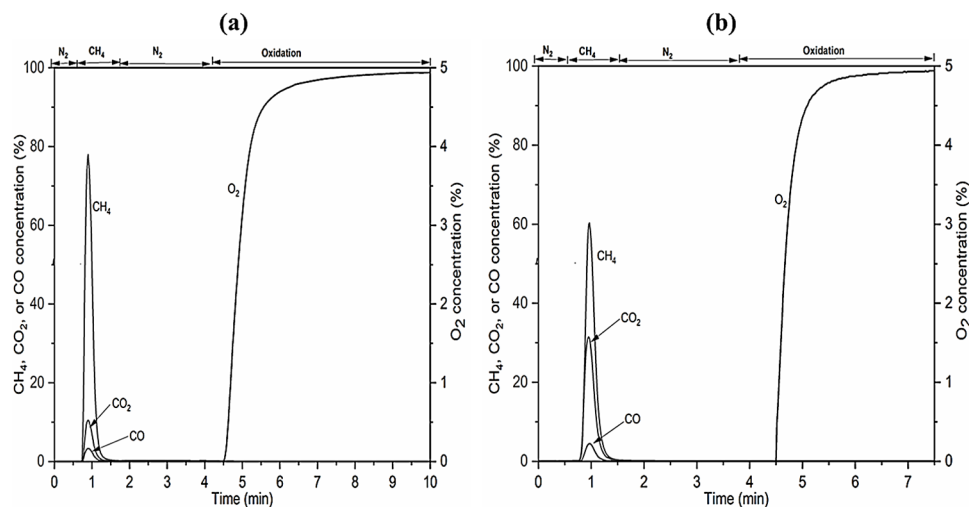
Figure 3. Concentration of CH_4, CO, CO_2, and O_2 as a function of time for a typical cycle of (a) CH_4 cycle (10th cycle in Na−K charcoal series) with calcined ilmenite oxygen carrier (b) CH_4 cycle (10th cycle in Na−K charcoal series) with synthetic ilmenite oxygen carrier at 950 °C.

The gas yield (γ) is defined as the ratio of fully oxidized fuel to carbon-containing gases in the outlet stream. When methane and syngas are used as fuels, the gas yield is calculated using eqs 4, 5, and 6. These parameters are represented by, γ_{CH_4}, γ_{H_2}, and γ_{CO}.

$$\gamma_{CH_4} = \frac{x_{CO_2}}{x_{CH_4} + x_{CO} + x_{CO_2}} \tag{4}$$

$$\gamma_{CO} = \frac{x_{CO_2}}{x_{CO} + x_{CO_2}} \tag{5}$$

$$\gamma_{H_2} = 1 - \frac{x_{H_2}}{x_{CO} + x_{CO_2}} \tag{6}$$

Here, x_i (i = CH_4, CO, CO_2) represents the concentration of the respective gas, measured in volume percentage (vol %), which is obtained from the gas analyzer.

3.2. Solid Fuels. The fraction of char conversion, $X_C(t)$, during a solid fuel experiment, is defined as

$$X_c(t) = \frac{m_c(t)}{m_{c,total}} \tag{7}$$

Here $m_C(t)$ corresponds to the amount of carbon that has undergone conversion at a given time t and $m_{C,total}$ represents the total cumulative carbon converted throughout a complete cycle. The determination of both $m_C(t)$ and $m_{C,total}$ involves integrating the concentrations of carbon-containing gases using eq 8.

$$m_c(t) = \int_{t_0}^{t} \dot{n}_{out} M_C (x_{CH_4} + x_{CO_2} + x_{CO}) dt \tag{8}$$

Here M_C denotes the molar mass of carbon, $\dot{n}_{out}$ represents the molar flow rate of dry gas at the reactor exit, determined by calibrating the flow readings from the gas analyzer, and x_i (where i = CH_4, CO, CO_2) represents the concentration of the respective gas, measured in volume percent (vol. %), as obtained from the gas analyzer.

The instantaneous rate of char gasification based on the remaining unreacted carbon in the bed, r_{inst}, is calculated using eq 9. The average rate of char gasification is determined by

calculating the arithmetic mean of the instantaneous rate of char gasification within a conversion (X_C) range of 0.3−0.7

$$r_{inst} = \frac{1}{(1 - X_C)} \frac{dX_C}{dt} \tag{9}$$

The gas conversion (η_{gas}) for solid fuels (charcoal, K-charcoal, Na-charcoal, and Na−K charcoal) represents the ratio of CO and H_2 transformed into CO_2 and H_2O during the reduction process, as calculated using eq 10. The average gas conversion value is determined by computing the arithmetic mean of the instantaneous gas conversion rates within a conversion (X_C) range of 0.3−0.7.

$$\eta_{gas} = 1 - \frac{0.5x_{co} + 0.5x_{H_2}}{x_{co_2} + x_{co}} \tag{10}$$

3.3. Pressure Fluctuation. The pressure fluctuations of the bed were monitored to determine whether the bed was fluidized during the experiments. The amplitude of the pressure fluctuations, denoted by σ, was determined using eq 11. Data from the middle part of the oxidation period were used to calculate σ. This middle period was chosen because it represents stable conditions, with no gas switching occurring. The oxidation data from this stage were divided into smaller groups of nine data points each. The average value of these data groups was then used to calculate σ, as described in eq 11.

$$\sigma = \frac{1}{N - m} \sum \left(\frac{1}{m} \cdot \sum_{j=i}^{i+m} \left(\Delta p_j - \Delta p_{avg} \right)^2 \right)^{1/2} \tag{11}$$

In the evaluation process, N represents the total number of pressure-drop values considered. For the selected analysis, the number of samples in each smaller group, denoted by m, was set to nine to obtain accurate fluctuation values. To calculate the amplitude (σ), the period under analysis was divided into numerous shorter periods. Within each of these shorter periods, the average value of the pressure drops, denoted as Δp_{avg}, was computed based on ($m + 1$) pressure-drop values, where m is 9 in this case. Δp_j is the jth individual pressure drop within a smaller group. A more reliable measure of σ was derived by averaging the amplitudes of these shorter periods.
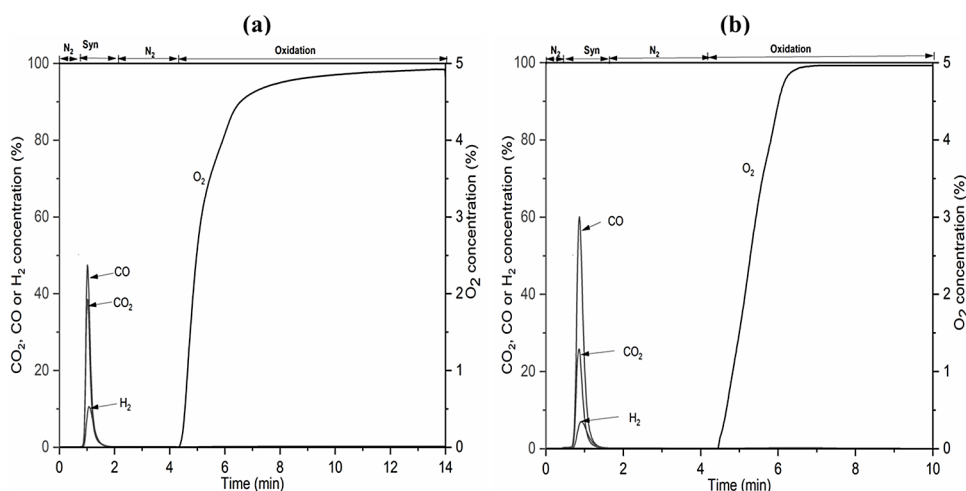
(a)   **(b)**

Figure 4. Concentration of CO_2, CO, H_2, and O_2 as a function of time for a typical cycle of (a) Syngas (10th Syngas cycle following the Na−K charcoal series) with used calcined ilmenite oxygen carrier and (b) Syngas (10th Syngas cycle following the Na−K charcoal series) with used synthetic ilmenite oxygen carrier at 950 °C.
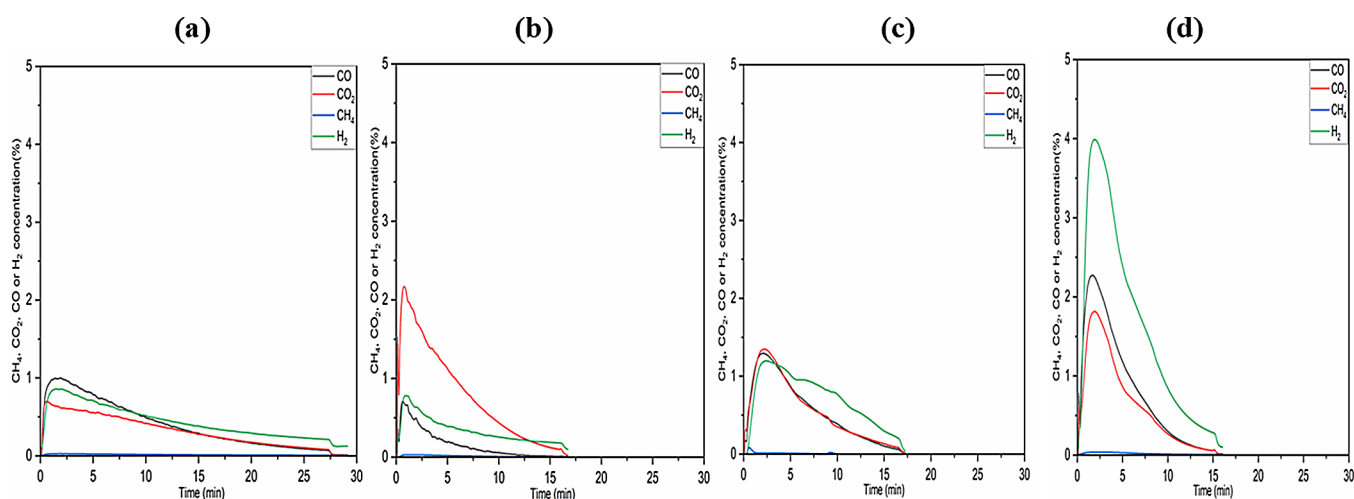
(a)   **(b)**   **(c)**   **(d)**

Figure 5. Concentration of CO_2, CO, and H_2 as a function of time for calcined ilmenite oxygen carrier reaction with (a) Charcoal (13th cycle in Na-charcoal series), (b) K-charcoal (39th cycle in K-charcoal series), (c) Na-charcoal (39th cycle in Na-charcoal series), and (d) Na−K charcoal (39th cycle in Na−K charcoal series) at 950 °C.

This approach was adopted because computing the amplitude over the entire time period could result in misleading results due to changes in the average value. Breaking down the time period into shorter segments helps capture more accurate and meaningful variations in the pressure fluctuations.

The state of fluidization can be determined by analyzing the magnitude of pressure fluctuations (σ). When the amplitude of the pressure fluctuations exceeds 0.04, it indicates a state of good fluidization. A σ value between 0.02 and 0.04 indicates a weak fluidization state, while a σ value below 0.02 implies a state of bed defluidization.

4. RESULTS AND DISCUSSION

4.1. Reaction with Methane and Syngas. Figure 3 and Figure 4 show typical cycles that involve methane cycle tests and syngas cycle tests. The cycle consists of the consecutive stages of reduction, denoted by "CH_4" or "Syn," inert marked as "N_2," and oxidation labeled as "Oxidation." The calcined ilmenite and synthetic ilmenite used in the methane test shown

in Figure 3a,b had not been exposed to any impregnated charcoal.

During the methane test with calcined ilmenite, the peak methane concentration reached approximately 78%, resulting in peak CO_2 and CO concentrations of 10.4 and 3.3%, respectively. In contrast, during the methane test with synthetic ilmenite, the peak methane concentration was around 60.4%, with peak CO_2 and CO concentrations of 31.5 and 4.5%, respectively. These values indicate moderate reactivity for calcined ilmenite and relatively high reactivity for synthetic ilmenite. Notably, the char was fully converted, as no carbonaceous gas was detected during the oxidation reaction.

Figures 4a,b illustrate typical cycles of syngas tests conducted with used calcined ilmenite and used synthetic ilmenite after the 60 cycles shown presented in Table 4. Compared to the methane cycles, a smaller quantity of ilmenite was used in the syngas: 2 g of ilmenite and 13 g of sand in the bed. During the reduction of used calcined ilmenite with syngas, the peak concentrations of CO and H_2 were around 47.5 and 10.5%, respectively, with the peak CO_2 concentration reaching 38.5%. Conversely, the reduction of used synthetic
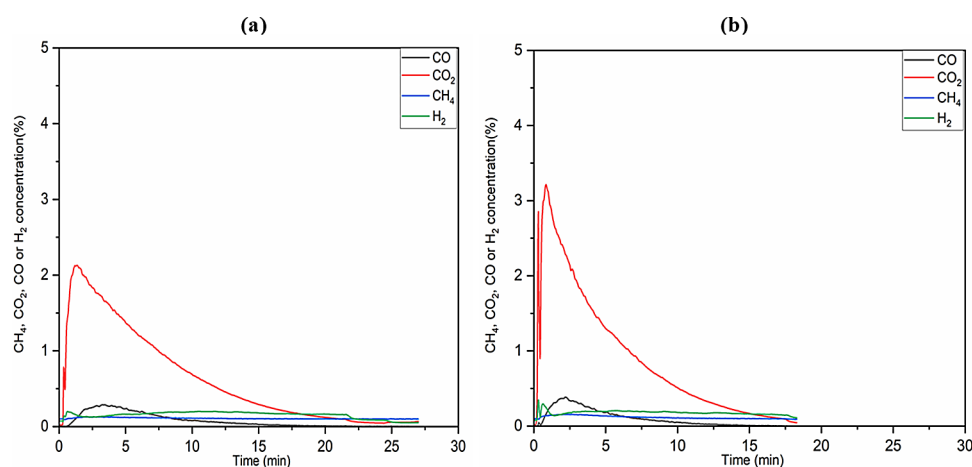
Figure 6. Concentration of CH_4, CO_2, CO, and H_2 as a function of time for synthetic ilmenite oxygen carrier reaction with (a) Charcoal (13th cycle) and (b) Na−K charcoal (59th cycle) at 950 °C.

ilmenite with syngas resulted in CO, H_2, and CO_2 concentrations of approximately 60.1, 7.0, and 25.8%, respectively. This decrease in the conversion of synthetic ilmenite is attributed to the reduction in the porosity due to the formation of a layer of alkali-silicate after exposure to alkali, leading to a decrease in the active sites for the chemical reaction with syngas. Conversely, the calcined ilmenite has more porosity and retained more active sites for the reaction with syngas after exposure to alkali, resulting in higher reactivity. Furthermore, the oxidation process of reduced calcined ilmenite with syngas required more time to achieve a steady O_2 concentration compared to used synthetic ilmenite.

4.2. Reaction with Solid Fuels. Figure 5 depicts the reduction periods for the four different types of solid fuels: charcoal, K-charcoal, Na-charcoal, and Na−K charcoal with calcined ilmenite. In the case of charcoal without alkali impregnation with calcined ilmenite, the main gas products were CO_2, CO, and H_2, with a very low concentration of CH_4. Complete gasification of charcoal is time-consuming, taking approximately 30 min, and exhibiting an extended tail of CO_2, CO, and H_2 in the gas composition. However, when the fuel was changed to K-charcoal, Na-charcoal, and Na−K charcoal, the concentrations of all gases (CO_2, CO, and H_2) were notably higher in the initial minutes, indicating a char gasification rate that was almost twice as fast. This acceleration in gasification is attributed to the catalytic effect of the alkali, as reported in previous studies.[22,23,51,52] In the case of Na−K-impregnated charcoal, the concentration of H_2 was significantly higher than that of CO_2 and CO. This phenomenon is likely a result of the water−gas shift reaction, which transforms CO and H_2O into CO_2 and H_2, respectively, under steam-rich conditions.[30]

Figure 6 presents the reduction periods using charcoal and Na−K charcoal with synthetic ilmenite. For charcoal without alkali impregnation combined with synthetic ilmenite, CO_2 is the main gas product, peaking at 2.2%, with minimal levels of CO, H_2, and CH_4. However, when using Na−K charcoal, the peak concentration of CO_2 rises to around 3.2%, while the concentrations of CO, H_2, and CH_4 remain unchanged. The gasification time for charcoal with synthetic ilmenite is slow, in contrast to the faster gasification with Na−K charcoal.

4.3. Rate of Char Gasification. Figure 7 illustrates the average gasification rate as a function of cycle number for different charcoal series: K-charcoal, Na-charcoal, Na−K
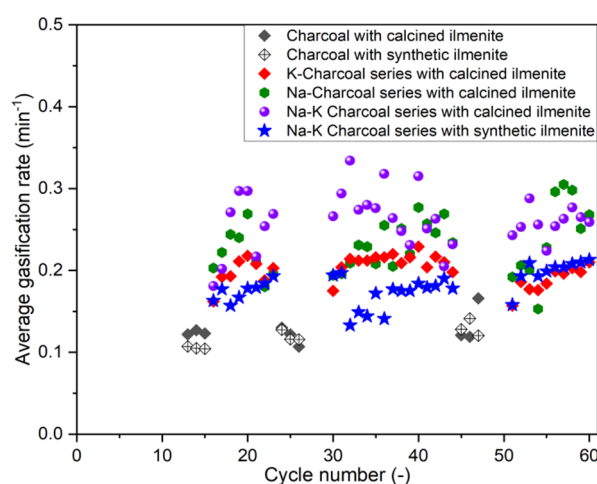

Figure 7. Rate of char gasification as a function of cycle number during the reduction period of charcoal with calcined and synthetic ilmenite, K-charcoal, Na-charcoal, and Na−K charcoal series with calcined ilmenite, and Na−K charcoal series with synthetic ilmenite.

charcoal with calcined ilmenite, and Na−K charcoal with synthetic ilmenite. The gasification rate was computed using eq 9, and average values were calculated within the range of X_C = 0.3−0.7 for comparative analysis, consistent with previous studies.[53,54] Charcoal exhibited gasification rates of 0.107− 0.166 min^{-1} with calcined ilmenite and 0.105−0.141 min^{-1} with synthetic ilmenite. The increased gasification rate observed in the K-charcoal, Na-charcoal, and Na−K charcoal series is ascribed to the catalytic impact of alkali.[23,25,52,55] The K-charcoal series demonstrated gasification rates ranging from 0.157 to 0.229 min^{-1} with calcined ilmenite, followed by the Na-charcoal series (0.096−0.305 min^{-1}). The Na−K charcoal series exhibited the highest gasification rate, ranging from 0.181 to 0.334 min^{-1} with calcined ilmenite. Conversely, the Na−K charcoal series with synthetic ilmenite manifested the lowest gasification rate within the range of 0.131−0.209 min^{-1} among the impregnated charcoal series, possibly because of the absence of materials facilitating char gasification present in calcined ilmenite. Interestingly, after 50 cycles, the average gasification rate of the Na−K charcoal series with synthetic ilmenite increased, reaching levels comparable to those of the K-charcoal series with calcined ilmenite. This phenomenon is
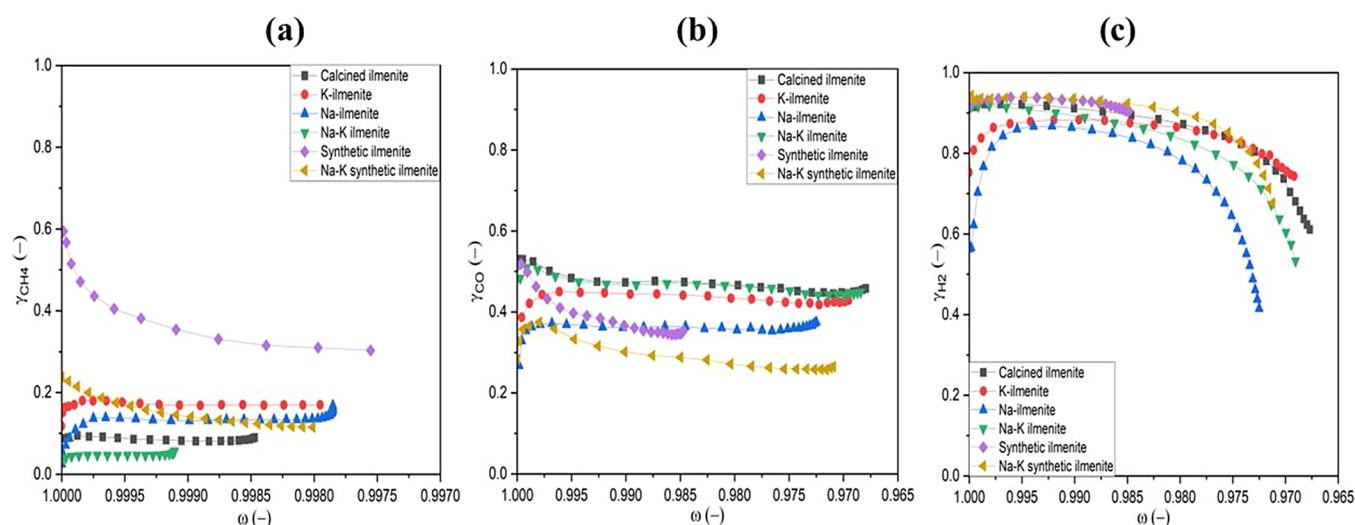
Figure 8. Gas yield from each gas component (a) CH_4 for calcined ilmenite (12th cycle in Na−K charcoal series), synthetic ilmenite (12th cycle in Na−K charcoal series), K-ilmenite (50th cycle in with calcined ilmenite), Na-ilmenite (50th cycle with calcined ilmenite), Na−K ilmenite (50th cycle with calcined ilmenite), and Na−K synthetic ilmenite (50th cycle). Syngas cycles (b) CO and (c) H_2 were made with 2g samples not cycled and samples taken after the 60 cycles in Table 4.
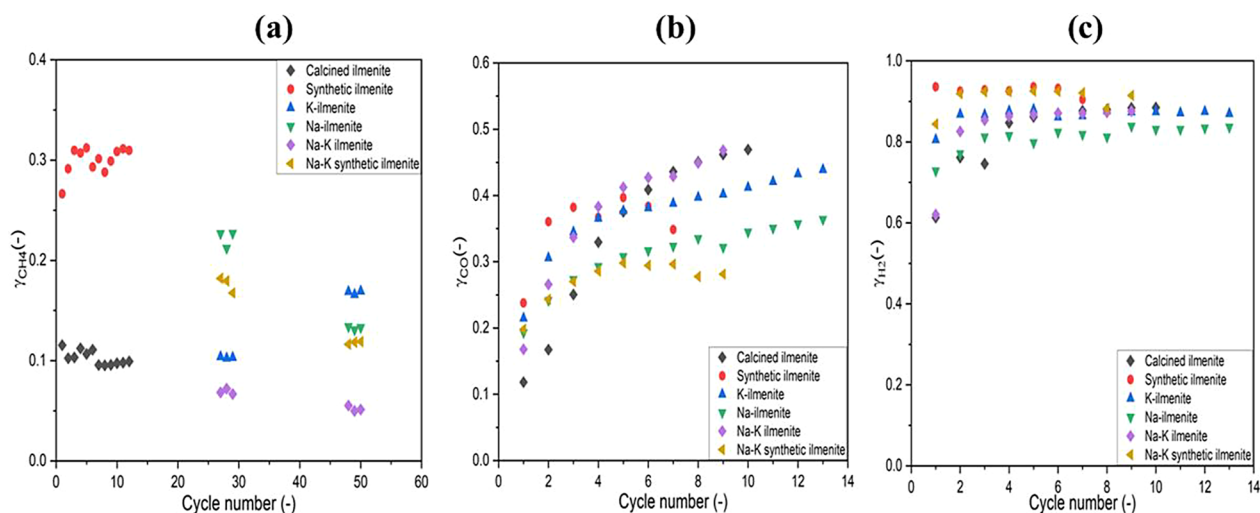

Figure 9. Gas yield vs cycle number for each gas component (a) CH_4, (b) CO, and (c) H_2 for calcined ilmenite, synthetic ilmenite, K-ilmenite, Na-ilmenite, Na−K ilmenite, and Na−K synthetic ilmenite. Data are from ω = 0.998 with CH_4 and 0.98 with syngas.

attributed to the absorption of alkali metals (Na and K) by synthetic ilmenite over the cycles, thereby catalyzing charcoal gasification.

4.4. Reactivity of Calcined, Synthetic, and Used Ilmenite. The reactivity of calcined, synthetic, and used ilmenite samples was investigated through exposure to methane and syngas, with examples shown in Figure 8. In the syngas cycles, 2 g of oxygen carrier was mixed with 13 g of inert material, i.e., silica sand. The syngas cycles were conducted with samples that had not been cycled with char, or samples taken after the full series of 60 cycles in Table 4

The gas yield (γ) of methane at ω = 0.998 and syngas (CO and H_2) at ω = 0.98 as a function of the cycle number is depicted in Figure 9. For methane interaction, synthetic ilmenite exhibited the highest reactivity during the initial cycle (1−12) before alkali cycling. However, after cycling with Na−K charcoal, the reactivity of synthetic ilmenite declined sharply, as shown in Figure 9a. Conversely, calcined ilmenite demonstrated moderate reactivity with methane, which was

altered after interaction with alkali charcoal. Following the interaction with Na−K charcoal, the reactivity of calcined ilmenite in the presence of methane decreased. The simultaneous presence of Na and K can mutually influence their behaviors. K can inhibit the mobility of Na by promoting the formation of a passive layer of sodium silicates on the ilmenite surface, thereby reducing the availability of free Na for reaction with ilmenite.[56] This passive layer can further inhibit reactions by obstructing the active sites on the ilmenite surface. Consequently, the reactivity of calcined ilmenite decreased following the reaction with Na−K charcoal in the presence of methane. After interacting with Na-charcoal, the reactivity of calcined ilmenite initially increased but then dropped due to the initial availability of free sodium. However, interaction with K-charcoal resulted in a distinct increase in reactivity after 47 cycles, attributed to the formation of K-titanate.[30]

For CO interaction, the reactivity of calcined ilmenite and used calcined ilmenite (K-ilmenite, Na-ilmenite, and Na−K charcoal) increased with the cycle number. This increase is

attributed to the presence of elemental iron in the reduction atmosphere.[30,57] Furthermore, the presence of K-titanates, which are more reactive than ilmenite, contributes to the enhanced reaction rate with CO.[30] In contrast, the reactivity of synthetic and Na−K synthetic ilmenite initially increased before declining. Nevertheless, synthetic ilmenite exhibited higher reactivity than Na−K synthetic ilmenite. This decline in the reactivity of Na−K synthetic ilmenite is due to the reduction in surface area and porosity resulting from the formation of an alkali-silicate layer after exposure to alkali. This reduction leads to fewer active sites available for the chemical reaction with CO. Conversely, synthetic ilmenite retained more active sites for the reaction with CO, thereby maintaining higher reactivity.

Regarding H_2 interaction, synthetic ilmenite, and Na−K synthetic ilmenite displayed the highest reactivity, which remained constant with increasing cycle numbers. Additionally, the reactivity of used ilmenite (K-ilmenite, Na-ilmenite, and Na−K ilmenite) also remained constant. However, the reactivity of calcined ilmenite increased with the cycle number.

4.5. Gas Conversion for Solid Fuels. Figure 10 demonstrates the gas conversion (η_{gas}) as a function of cycle
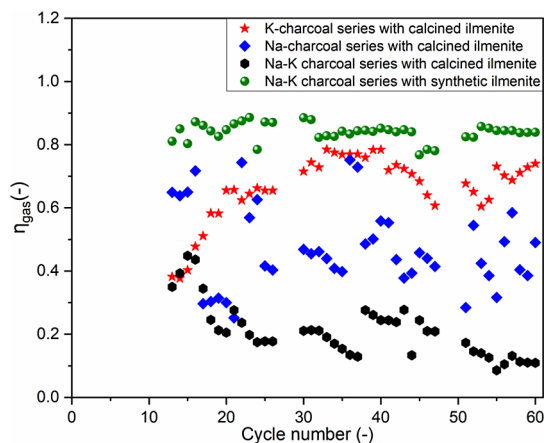

Figure 10. Gas conversion (η_{gas}) as a function of cycle number for K-charcoal series, Na-charcoal series, and Na−K charcoal series with calcined ilmenite and Na−K charcoal series with synthetic ilmenite.

number for K-charcoal, Na-charcoal, and Na−K charcoal series with calcined ilmenite, as well as the Na−K charcoal series with synthetic ilmenite. The gas conversion (η_{gas}) was determined utilizing eq 10, with the average values determined within the range of $X_C = 0.3-0.7$ for comparative analysis, consistent with previous studies.[25] The Na−K charcoal series with synthetic ilmenite exhibited the highest gas conversion, ranging from 0.70 to 0.89, followed by the K-charcoal series (0.38−0.78), and the Na-charcoal series (0.25−0.75) with calcined ilmenite. In contrast, the Na−K charcoal series with calcined ilmenite demonstrated the lowest gas conversion, ranging from 0.09 to 0.45 among the impregnated charcoal series tested. This suggests that the interaction between the gasification products (CO and H_2) and the bed material is most pronounced in the case of the Na−K charcoal with synthetic ilmenite bed material and least pronounced in the case of the Na−K charcoal with calcined ilmenite as bed material.

4.6. Pressure Drops Fluctuation Amplitude. The fluidization of the ilmenite bed was monitored by measuring

the amplitude of pressure drop fluctuations (σ) across the reactor tubes. Figure 11 presents the σ values as a function of
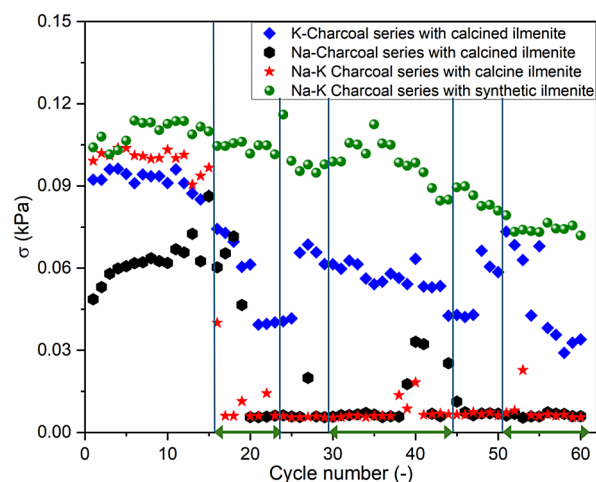

Figure 11. Amplitude of pressure drop fluctuations (σ) as a function of cycle number in the K- charcoal, Na-charcoal, and Na−K charcoal series with calcined ilmenite and Na−K charcoal series with synthetic ilmenite. Green arrows indicate cycles with alkali addition.

cycle number for four charcoal series: K-charcoal, Na-charcoal, Na−K charcoal with calcined ilmenite, and Na−K charcoal with synthetic ilmenite. In the initial 12 cycles using methane, the fluctuation amplitudes ranged from 0.04 to 0.12, indicating good fluidization. Differences in these amplitudes are attributed to different reactor tubes used for each series, potentially resulting in varying gas distributor porosities. In cycles 13−15, involving charcoal with calcined and synthetic ilmenite, the fluctuation amplitudes remained within the same range, indicating continued good fluidization. However, after 16 cycles, a sudden decrease in amplitude was observed for the Na−K charcoal series with calcined ilmenite, with the fluctuation amplitude dropping below 0.02, indicating a defluidization state. Some fluidization was noted in cycles 40 and 53, with fluidization amplitudes in the range of 0.02 to 0.04. Similarly, the Na-charcoal series with calcined ilmenite exhibited a decrease in fluctuation amplitude below 0.02 after cycle 19, indicating a defluidization state. Some fluidization was observed in cycles 27, 39, 40, 41, and 44, with amplitudes in the range of 0.02−0.04. For the K-charcoal series with calcined ilmenite, fluctuation amplitudes ranged from 0.02 to 0.08 during cycles 16−60, indicating fluidization, albeit with some periods of weaker fluidization, e.g., in cycles 56−60, with amplitudes in the range of 0.02−0.04. The higher volatility of KCl compared to NaCl resulted in greater KCl evaporation from the bed,[58] reducing its impact on agglomeration and defluidization during cycles 16−60 in the K-charcoal series with calcined ilmenite. This observation is supported by the ICP-SFMS analysis presented in Tables 3 and 5. In contrast, the Na−K charcoal series with synthetic ilmenite exhibited good fluidization in all cycles 16−60, although a slight decrease in pressure drop fluctuation amplitude was noted with increasing cycle number.

4.7. Agglomeration and Morphology of Ilmenite Particles. *4.7.1. Agglomeration Characteristics of Ilmenite.* Most of the ilmenite particles present in the bed did not form agglomerations, with only a small fraction combining to form agglomerates. The agglomerates varied in size, with dimensions

Table 5. Amount of Alkalis Added and Present in the Ilmenite and Synthetic Ilmenite Bed

|	K from K-charcoal series with calcined ilmenite	Na from Na-charcoal series with calcined ilmenite	K from Na−K charcoal series with calcined ilmenite	Na from Na−K charcoal series with calcined ilmenite	K from Na−K charcoal series with synthetic ilmenite	Na from Na−K charcoal series with synthetic ilmenite
alkali present in the calcined ilmenite (g)	0.062	0.010	0.062	0.010	<0.004	<0.004
alkali added until middle cycle (g)	0.094	0.099	0.051	0.038	0.117	0.087
alkali present after middle cycle (g)	0.128	0.080	0.028	0.038	0.050	0.044
alkali retention after middle cycle (g)	0.066	0.070	−0.034	0.028	0.046	0.040
$\frac{\text{Alkali retention}}{\text{Alkali added}} \times 100$ until middle cycle	70.21	70.71	−66.67	73.68	39.32	45.98
total alkali added in all cycles (g)	0.172	0.172	0.168	0.125	0.168	0.125
alkali present after final cycle (g)	0.110	0.094	0.044	0.060	0.062	0.054
alkali retention after final cycle (g)	0.048	0.084	−0.018	0.050	0.058	0.050
$\frac{\text{Alkali retention}}{\text{Total alkali added}} \times 100$	27.91	48.84	−10.71	40.00	34.52	40.00
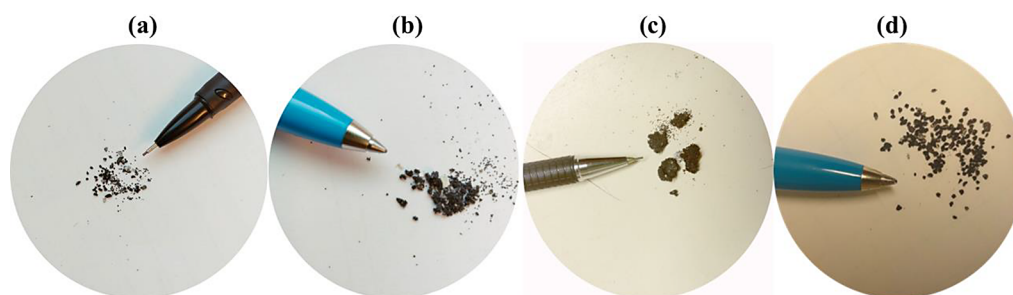
Figure 12. Agglomeration of calcined ilmenite using (a) K-charcoal, (b) Na-charcoal, (c) Na−K charcoal and synthetic ilmenite using (d) Na−K charcoal after 33 alkali oxidation−reduction cycles.
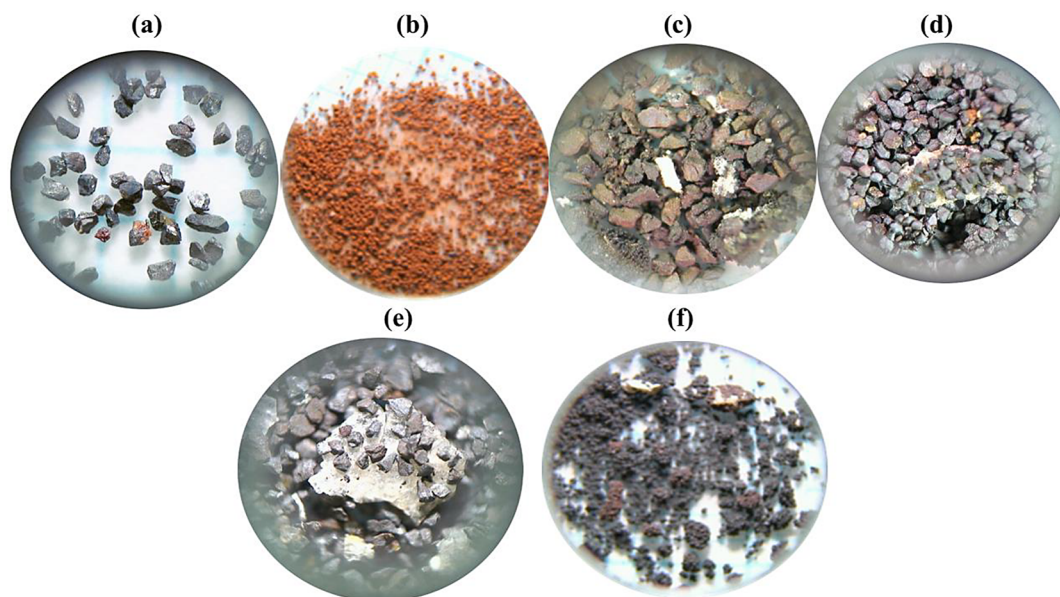

Figure 13. Light microscope images of (a) Calcined ilmenite, (b) Synthetic ilmenite, (c) K-ilmenite, (d) Na-ilmenite, (e) Na−K ilmenite, and (f) Na−K synthetic ilmenite.

of 0.5−1 mm for K-ilmenite, 2−3 mm for Na-ilmenite, 3−5 mm for Na−K ilmenite, and 1−2 mm for Na−K synthetic ilmenite, as depicted in Figure 12. These agglomerates were structurally weak and easily fragmented. Consequently, during the experiments involving K-charcoal and calcined ilmenite, as well as Na−K charcoal and synthetic ilmenite, minimal to no agglomeration was observed in the ilmenite bed. In contrast, experiments with Na-charcoal and Na−K charcoal combined

with calcined ilmenite demonstrated a higher degree of bed agglomeration.

4.7.2. Morphology of Ilmenite Particles. 4.7.2.1. Light Microscope Images. Light microscope images of calcined ilmenite, synthetic ilmenite, and final samples of K-ilmenite, Na-ilmenite, Na−K ilmenite, and Na−K synthetic ilmenite are shown in Figure 13. The particles exhibit different colors, such as brown and gray, in contrast to the uniform black dispersion of calcined ilmenite. Synthetic ilmenite appears orange with uniform distribution. K-ilmenite final particles are brown, Na-ilmenite final particles are light orange, Na−K ilmenite final particles are gray, and Na−K synthetic ilmenite particles are brown. Molten particles are observed on the surfaces of Na-ilmenite and Na−K ilmenite samples. The agglomerated particles can be easily separated by hand, and they do not form hard agglomerates within the ilmenite structure, making them easy to break apart.

4.7.2.2. SEM-EDX. To examine the changes in the morphology and elemental distribution within the particles, a cross-sectional analysis of the particles was conducted using scanning electron microscopy and energy-dispersive X-ray spectroscopy (SEM-EDX). The samples were embedded in epoxy and polished for analysis. The K-ilmenite, Na-ilmenite, Na−K ilmenite, and Na−K synthetic ilmenite particles after the final cycles were examined using SEM-EDX to determine the interactions of K and Na with the ilmenite and synthetic ilmenite particles, as shown in Figure 14.

In the calcined ilmenite sample, iron (Fe) and titanium (Ti) are evenly distributed and thoroughly separated among the distinct particles, although these results are not presented here. In the final samples of K-ilmenite, Na-ilmenite, and Na−K ilmenite, the distributions of Fe and Ti remained consistent, with particles well-dispersed and separated across all samples. However, Fe and Ti were absent from the bridges between particles in these samples, indicating that Fe and Ti do not significantly contribute to agglomeration. The agglomeration mechanism differed among the K-ilmenite, Na-ilmenite, and Na−K ilmenite samples. EDX analysis of K-ilmenite confirmed the absence of K in the Si and Al bridges. In contrast, Na was detected in the bridges of Na-ilmenite, where Na, Al, and Si combined to form a distinct agglomeration. In Na−K ilmenite, both Na and K were found in the bridges with Si and Al, leading to agglomeration due to the combination of these elements. The presence of Na and K in the bridges was notably higher compared to single-impregnated charcoal. In the Na−K synthetic ilmenite, EDX analysis showed no distinct accumulations of Na and K. However, Fe and Ti were evenly distributed and thoroughly separated among the distinct particles. Si was present inside or on the surface of particles, likely originating from the charcoal particles and appearing in small patches. A possible correlation of Si and Al with K and Na was observed on the surface of the particles.

Silicon significantly exacerbates ash agglomeration at moderate to high combustion temperatures when combined with alkali chlorides. This occurs because alkali chlorides react with silica to form alkali silicates,[56] which can melt or soften at relatively low temperatures, depending on the specific alkali involved. These alkali-silica interactions promote the formation of bridges between particles in ilmenite agglomerates. However, the introduction of steam significantly alters the chemistry, particularly for KCl, which reacts with steam to form volatile KOH that partially evaporates.[30] KOH further reacts with ilmenite, forming K-titanate. Unlike NaCl, KCl
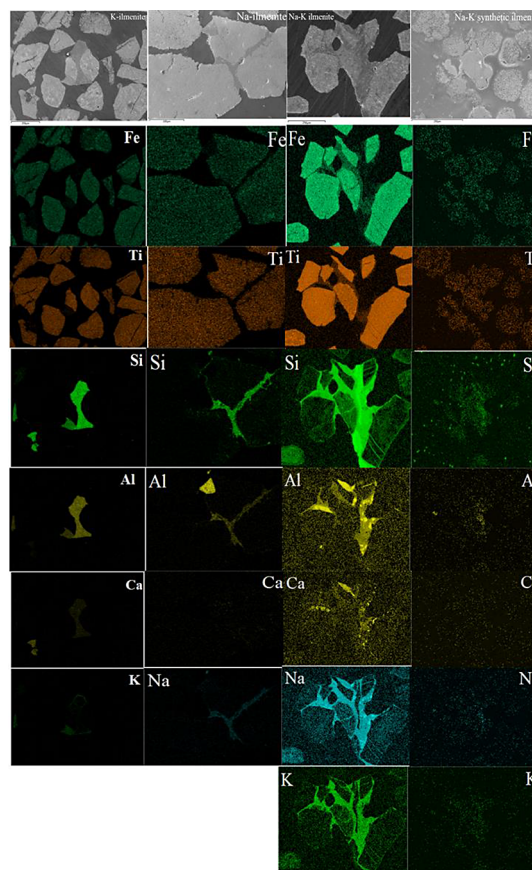

Figure 14. SEM-EDX analyses of the cross sections of agglomerates of the K-ilmenite, Na-ilmenite, Na−K ilmenite, and Na−K synthetic ilmenite particles after the final cycle with alkali fuel. Elements Fe, Ti, Si, Al, Ca, Na, and K on the cross sections of the particles are presented for evaluation and comparison.

tends to volatilize and escape to the reactor wall rather than remaining in the bed to react with ilmenite.[58,59] As a result, no K was observed in the bridges between particles in K-ilmenite agglomerates. In contrast, Na is present in the bridges between particles in Na-ilmenite agglomerates. NaCl reacts with ilmenite and silica particles to form the Na_2O_5SiTi phase in the presence of steam. However, the formation of K-titanate and Na_2O_5SiTi phases is limited due to the insufficient availability of steam at the relatively high reaction temperatures. Additionally, other mineral components such as Al, influence agglomeration, as metal chloride molecules tend to be absorbed into Al sites. In Na−K ilmenite, the concentration of Na and K in these bridges is significantly higher compared to single-impregnated charcoal, leading to larger agglomerates. This is because K inhibits the release of Na, thereby promoting agglomerate formation.[56] Conversely, in the interaction between Na−K charcoal and synthetic ilmenite, the agglomerate size was relatively smaller due to the absence of Si in the synthetic ilmenite. Here, Si originates from the Na−K charcoal and interacts with the sodium and potassium present in the Na−K charcoal.

4.8. Analysis of Crystalline Phases. X-ray diffraction (XRD) analysis was performed to characterize the crystalline phases present in the various ilmenite samples, aiming to elucidate the phase transformations these materials undergo. The samples analyzed included calcined ilmenite, synthetic ilmenite, and final samples of Na-ilmenite, K-ilmenite, Na−K

ilmenite, and Na−K synthetic ilmenite. After the final reduction phase, the samples were cooled in a nitrogen atmosphere, and the XRD profiles are shown in Figure 15.
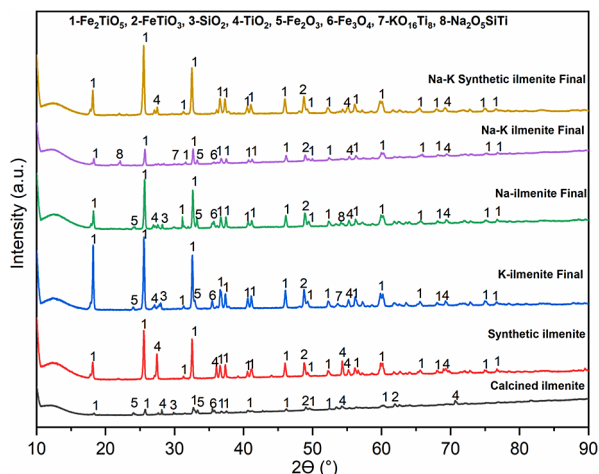

Figure 15. XRD patterns of the calcined ilmenite, synthetic ilmenite, K-ilmenite final, Na-ilmenite final, Na−K ilmenite final, and Na−K synthetic ilmenite final.

In their reduced state, XRD analysis identified the presence of magnetite (Fe_3O_4) and ilmenite ($FeTiO_3$), which are the reduced forms of hematite (Fe_2O_3) and pseudobrookite (Fe_2TiO_5), respectively. Despite the reduction process, residual phases of hematite (Fe_2O_3) and pseudobrookite (Fe_2TiO_5) were detected, indicating incomplete conversion. Additionally, rutile (TiO_2) was observed, likely forming through the oxidation of ilmenite to Fe_2O_3 and pseudobrookite.[60] Silica (SiO_2) was also present in calcined ilmenite and used calcined ilmenite samples. XRD analysis of the final K-ilmenite and Na−K ilmenite samples revealed the presence of various potassium titanate phases, specifically KTi_8O_{16} and $K_{1.28}Ti_8O_{16}$, suggesting a mixture of different K-titanate compounds. Figure 15 illustrates the best-fitting compound, confirming the detection of KTi_8O_{16}, which aligns with previous studies.[30,61] Conversely, XRD analysis of the final Na-ilmenite samples identified the Na_2O_5SiTi phase, which resulted from the reaction between Na-impregnated charcoal and the Si and Ti phases in ilmenite. The final Na−K ilmenite samples exhibited a combination of various K-titanate phases and Na_2O_5SiTi. For the final Na−K synthetic ilmenite sample, XRD analysis identified the presence of $FeTiO_3$, TiO_2, and Fe_2TiO_5, but K-titanate and Na_2O_5SiTi phases were not detected.

4.9. Alkali Retention in the Ilmenite Bed. The estimation of alkali retention by both calcined and synthetic ilmenite during multiple oxidation−reduction cycles was determined by measuring the difference in alkali content of ilmenite before and after the operation.[62] The retained quantities of potassium (K) and sodium (Na) after the middle and final cycles were compared with the theoretical amount of alkali introduced into the ilmenite bed, as detailed in Table 5. The calculations for the retained K and Na were conducted using ICP-SFMS analyses of samples collected after the middle and final cycles.

In the K-charcoal series, 0.172 g of K was introduced to the calcined ilmenite bed. Similarly, 0.172 g of Na was added to the calcined ilmenite bed in the Na-charcoal series. In the Na−

K charcoal series involving both calcined ilmenite and synthetic ilmenite, 0.168 g of K and 0.125 g of Na were added to the respective beds. These quantities correspond to 0.86, 0.86, 0.84, and 0.63% of the total weight of the ilmenite bed, respectively.

The percentage of K and Na retention exhibited a notable surge during the middle cycle, peaking at 70 and 71%, respectively, before declining to 28 and 49% after the final cycles in the K-charcoal and Na-charcoal series with calcined ilmenite. Conversely, in the Na−K charcoal series with calcined ilmenite, the percentage of K retention dropped by 67% during the middle cycle, subsequently increasing to −11%, while the percentage of Na retention escalated to 74% in the middle cycle before receding to 40% after the final cycles. In the Na−K charcoal series with synthetic ilmenite, the percentage of K retention rose to 39% during the middle cycle before declining to 35%, whereas the percentage of Na retention increased to 46% in the middle cycle and subsequently decreased to 40% after the final cycles.

The observed phenomena can be elucidated by the inherent characteristics of alkali binding to calcined ilmenite particles across multiple oxidation−reduction cycles. This pattern is primarily ascribed to the weak binding affinity between alkali ions and calcined ilmenite particles. Consequently, alkali ions, particularly potassium (K) ions, tend to evaporate from the calcined ilmenite bed and adhere to the reactor wall due to their loosely bound nature. Analyses reveal that the calcined ilmenite bed retains a notably higher percentage of sodium ions (Na) compared to potassium ions (K), suggesting that sodium ions (Na) have a greater affinity for interaction with the silicon (Si) and aluminum (Al) components present within the bed, in contrast to potassium ions (K). The series with Na−K charcoal and calcined ilmenite deviates from this trend, showing a negative retention of potassium ions (K), indicating not only the loss of added potassium ions (K) but also a loss of potassium ions (K) already present in the ilmenite. A comparison of the potassium ions (K) content in calcined ilmenite, Na-ilmenite middle, and Na-ilmenite final samples (as shown in Table 3) reveals a gradual loss of potassium ions (K) in the Na-charcoal series. The quantities of introduced and retained alkali ions are further illustrated in Figure 16.
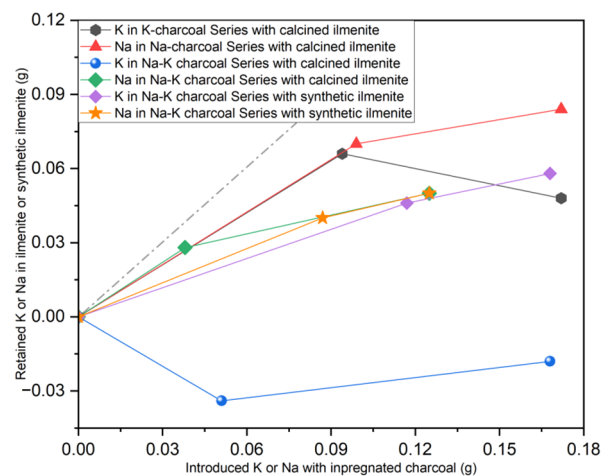

Figure 16. Retention of K and Na in the ilmenite as a function of the cumulative amount of K and Na introduced with the solid fuels. Dashed line shows 100% retention for comparison.

5. CONCLUSIONS

This research investigated the interactions between alkali chlorides (KCl and NaCl) and both natural and synthetic ilmenite. Experiments were conducted in a batch fluidized bed reactor using charcoal and three types of impregnated charcoal (K-charcoal, Na-charcoal, and Na−K charcoal), along with gaseous fuels (methane and syngas). The Na−K charcoal exhibited the highest gasification rate, followed by the Na-charcoal series, and then the K-charcoal series with calcined ilmenite. In contrast, the Na−K charcoal with synthetic ilmenite demonstrated the lowest gasification rate among the impregnated charcoal series. Gasification rates with unimpregnated charcoal were notably lower for both calcined and synthetic ilmenite. Regarding gas conversion (η_{gas}), no definitive conclusion could be drawn about the effect of alkali addition, although K appeared to be more effective than Na. Additionally, the redox cycling of the material itself may also have influenced the behavior of the oxygen carrier. The Na−K charcoal series combined with calcined ilmenite showed earlier agglomeration and defluidization compared to the Na-charcoal series while cycling with K-charcoal and calcined ilmenite led to only partial defluidization. Notably, no defluidization was observed during the 60 oxidation−reduction cycles with the Na−K charcoal series using synthetic ilmenite.

The XRD analyses of final samples, including K-ilmenite, Na-ilmenite, Na−K ilmenite, and Na−K synthetic ilmenite, demonstrated the interactions between alkali chlorides and ilmenite. KCl-impregnated charcoal reacted with calcined ilmenite, resulting in the formation of various K-titanate phases. In contrast, NaCl-impregnated charcoal interacted with both Si and Ti phases present in ilmenite, leading to the formation of the Na_2O_5SiTi compound. Reactions involving NaCl and KCl-impregnated charcoal with ilmenite revealed the presence of both K-titanate and Na_2O_5SiTi phases. However, no K-titanate or Na_2O_5SiTi phases were detected during the cycles with the Na−K charcoal series with synthetic ilmenite. The EDX analysis of K-ilmenite showed no K accumulation in the bridges between Si and Al elements within the Fe−Ti rich phases (Figure 12a). Conversely, Na-ilmenite exhibited a slight accumulation of Na in the bridges, with Na, Al, and Si forming distinct agglomerates (Figure 12b). In Na−K ilmenite, both Na and K, along with Si and Al, were prominently present in the bridges, leading to agglomeration due to the combined presence of K, Na, Si, and Al (Figure 12c). The combined effect of Na and K was more pronounced compared to the effects observed with single-impregnated charcoal. In contrast, EDX analysis of Na−K charcoal with synthetic ilmenite revealed no significant accumulation of Na and K in any bridges. Fe and Ti are evenly distributed and well-separated among distinct particles, while Si from charcoal particles appeared in small, dispersed patches. Consequently, it can be concluded that agglomerations observed in calcined ilmenite in the presence of Na and K are associated with the presence of Si in ilmenite.

The K and Na were introduced into the calcined ilmenite bed through the use of K-charcoal, Na-charcoal, and Na−K charcoal series, and these elements were partially retained in the bed material. After the final set of cycles, approximately 28% of K and 49% of Na were retained in the K-charcoal and Na-charcoal series, respectively. However, in the Na−K charcoal series, the results from the final cycle indicated a negative retention of K, with only 40% retention of Na,

suggesting a loss of K from the calcined ilmenite. In the Na−K charcoal series with synthetic ilmenite, retention percentages after the final cycles were 35% for K and 40% for Na.

Overall, the results of this research significantly enhance our understanding of the interactions between alkali chlorides and ilmenite, providing valuable insights that could influence future studies and practical applications in related fields.

■ AUTHOR INFORMATION

Corresponding Author

Ashwani Kumar Dubey − *Division of Energy Technology, Department of Space, Earth and Environment, Chalmers University of Technology, 41296 Gothenburg, Sweden;* ● orcid.org/0000-0002-2787-0415; Email: ashwanid@chalmers.se

Authors

Daofeng Mei − *Division of Energy Technology, Department of Space, Earth and Environment, Chalmers University of Technology, 41296 Gothenburg, Sweden; Instituto de Carboquímica, Consejo Superior de Investigaciones Científicas (ICB-CSIC), 50018 Zaragoza, Spain;* ● orcid.org/0000-0001-8597-1903

Anders Lyngfelt − *Division of Energy Technology, Department of Space, Earth and Environment, Chalmers University of Technology, 41296 Gothenburg, Sweden;* ● orcid.org/0000-0002-9561-6574

Tobias Mattisson − *Division of Energy Technology, Department of Space, Earth and Environment, Chalmers University of Technology, 41296 Gothenburg, Sweden;* ● orcid.org/0000-0003-3942-7434

Henrik Leion − *Energy and Materials, Department of Chemistry and Chemical Engineering, Chalmers University of Technology, 41258 Gothenburg, Sweden*

Complete contact information is available at:
https://pubs.acs.org/10.1021/acs.energyfuels.4c02968

Notes

■ NOMENCLATURE

AR	air reactor
BECCS	bioenergy carbon capture and storage
calcined ilmenite	calcined natural ilmenite before any experiment
CCS	carbon capture and storage
CLC	chemical looping combustion
FR	fuel reactor
ICP-SFMS	inductively coupled plasma-sector field mass spectrometry

IPCC	Intergovernmental Panel on Climate Change
ISO	International Organization of Standardization
K-charcoal	charcoal impregnated with KCl
K-ilmenite	ilmenite sample taken after the final cycle in K-charcoal series with calcined ilmenite
K-ilmenite middle	ilmenite sample taken after middle cycles in K-charcoal series with calcined ilmenite
m	number of samples in each smaller group for the calculation of σ value
m_C (t)	total mass of carbon leaving the reactor at the time t (g)
$m_{C,\ total}$	total mass of carbon measured during the entire reduction with solid fuel (g)
m_{ox}	amount of ilmenite oxygen carrier used in the experiments (g)
M_C	molar mass of atomic carbon (g/mol)
M_O	molar mass of atomic oxygen (g/mol)
M_xO_y	oxygen carrier in the oxidized form
M_xO_{y-1}	oxygen carrier in the reduced form
n	nth number of the N pressure drop values
N	number of points used for the calculation of σ value
Na-charcoal	charcoal impregnated with NaCl
Na-ilmenite	ilmenite sample taken after final cycle in Na-charcoal series with calcined ilmenite
Na-ilmenite middle	ilmenite sample taken after middle cycle in Na-charcoal series with calcine ilmenite
Na−K charcoal	charcoal impregnated with both NaCl and KCl
Na−K ilmenite	ilmenite sample taken after final cycle in Na−K charcoal series with calcined ilmenite
Na−K ilmenite middle	ilmenite sample taken after middle cycle in Na−K charcoal series with calcined ilmenite
Na−K synthetic ilmenite	synthetic ilmenite sample taken after final cycle in Na−K charcoal series with synthetic ilmenite
Na−K synthetic ilmenite middle	synthetic ilmenite sample taken after middle cycle in Na−K charcoal series with synthetic ilmenite
r_{inst}	instantaneous rate of char gasification (min^{-1})
SEM-EDX	scanning electron microscopy-energy dispersive X-ray spectroscopy
synthetic ilmenite	synthetic ilmenite before any experiment
t	instantaneous reaction time (s)
t_0	time at the beginning of reduction (s)
x_i	dry gas concentrations of gas i (i = CH$_4$, CO, CO$_2$, or H$_2$)
X_C	carbon conversion in the solid fuels
XRD	X-ray diffraction
$\dot{n}_{out}$	molar flow rate of gas passing through the gas analyzer (mol/s)
η_{gas}	gas conversion for solid fuels (charcoal, K-charcoal, Na-charcoal, and Na−K charcoal)
Δp_j	jth individual pressure drop value over the bed (kPa)
Δp_{avg}	average of N pressure drop values (kPa)
σ	amplitude of pressure drop fluctuation
γ_i	gas yield for component i (i = CH$_4$, CO, and H$_2$) in the reaction with methane (CH$_4$) or syngas
ω_i	mass-based oxygen carrier conversion in the reduction with gas CH$_4$ (i = CH$_4$) or syngas (i = syn)

■ REFERENCES

(1) Pörtner, H.-O.; Roberts, D. C.; Tignor, M. M. B.; Poloczanska, E.; Mintenbeck, K.; Alegría, A.; Craig, M.; Langsdorf, S.; Löschke, S.; Möller, V.; Okem, A.; Rama, B. *Climate Change 2022: Impacts, Adaptation, and Vulnerability*. Contribution of Working Group II to the Sixth Assessment Report of the Intergovernmental Panel on Climate Change (IPCC), Cambridge University Press: Cambridge, U.K. and New York, 2022. https://report.ipcc.ch/ar6/wg2/IPCC_AR6_WGII_FullReport.pdf (Accessed 2024-06-05).

(2) Haszeldine, R. S. Carbon capture and storage: how can black be? *Science* **2009**, *325* (5948), 1647−1652.

(3) Boot-Handford, M. E.; Abanades, J. C.; Anthony, E. J.; Blunt, M. J.; Brandani, S.; Mac Dowell, N.; Fernandez, J. R.; Ferrari, M.-C.; Gross, R.; Hallett, J. P.; Haszeldine, R. S.; Heptonstall, P.; Lyngfelt, A.; Makuch, Z.; Mangano, E.; Porter, R. T. J.; Pourkashanian, M.; Rochelle, G. T.; Shah, N.; Yao, G. J.; Fennell, P. S. Carbon capture and storage update. *Energy Environ. Sci.* **2014**, *7*, 130−189.

(4) Adánez, J.; Abad, A.; García-Labiano, F.; Gayán, P.; de Diego, L. F. Progress in chemical-looping combustion and reforming technologies. *Prog. Energy Combust. Sci.* **2012**, *38*, 215−282.

(5) Adánez, J.; Abad, A.; Mendiara, T.; Gayán, P.; de Diego, L. F.; García-Labiano, F. Chemical looping combustion of solid fuels. *Prog. Energy Combust. Sci.* **2018**, *65*, 6−66.

(6) Lyngfelt, A. Chemical Looping Combustion: Status and Development Challenges. *Energy Fuel* **2020**, *34*, 9077−9093.

(7) Coppola, A.; Scala, F. Chemical Looping for Combustion of Solid Biomass: A Review. *Energy Fuels* **2021**, *35*, 19248−19265.

(8) Giuliano, A. D.; Capone, S.; Anatone, M.; Gallucci, K. Chemical looping combustion and gasification: A review and a focus on European research projects. *Ind. Eng. Chem. Res.* **2022**, *61*, 14403−14432.

(9) Goel, A.; Moghaddam, E. M.; Liu, W.; He, C.; Konttinen, J. Biomass chemical looping gasification for high-quality syngas: A critical review and technological outlooks. *Energ Convers Manage* **2022**, *268*, No. 116020.

(10) Lyngfelt, A.; Hedayati, A.; Augustsson, E. Fate of NO and Ammonia in Chemical Looping Combustion-Investigation in a 300 W Chemical Looping Combustion Reactor System. *Energy Fuels* **2022**, *36*, 9628−9647.

(11) Hildor, F.; Leion, H.; Linderholm, C. J.; Mattisson, T. Steel converter slag as an oxygen carrier for chemical-looping gasification. *Fuel Process. Technol.* **2020**, *210*, No. 106576.

(12) Mattisson, T.; Keller, M.; Linderholm, C.; Moldenhauer, P.; Ryden, M.; Leion, H.; Lyngfelt, A. Chemical-Looping Technologies Using Circulating Fluidized Bed Systems: Status of Development. *Fuel Process. Technol.* **2018**, *172*, 1−12.

(13) Pröll, T.; Lyngfelt, A. Steam Methane Reforming with Chemical-Looping Combustion − Scaling of Fluidized Bed-Heated Reformer Tubes. *Energy Fuels* **2022**, *36*, 9502−9512.

(14) Lyngfelt, A.; Leckner, B. A 1000 MWth Boiler for Chemical-Looping Combustion of Solid Fuels - Discussion of Design and Costs. *Applied Energy* **2015**, *157*, 475−487.

(15) Lyngfelt, A.; Pallarés, D.; Linderholm, C.; Lind, F.; Thunman, H.; Leckner, B. Achieving Adequate Circulation in Chemical-Looping Combustion − Design Proposal for a 200 MWth CLC Boiler. *Energy Fuels* **2022**, *36*, 9588−9615.

(16) Abad, A.; Adánez, J.; Gayán, P.; de Diego, L. F.; García-Labiano, F.; Sprachmann, G. Conceptual design of a 100 MWth CLC unit for solid fuel combustion. *Applied Energy* **2015**, *157*, 462−474.

(17) Leion, H.; Lyngfelt, A.; Johansson, M.; Jerndal, E.; Mattisson, T. The use of ilmenite as an oxygen carrier in chemical-looping combustion. *Chem. Eng. Res. Des.* **2008**, *86*, 1017−1026.

(18) Matzen, M.; Pinkerton, J.; Wang, X.; Demirel, Y. Use of natural ores as oxygen carriers in chemical looping combustion: A review. *Int. J. Greenh. Gas Control.* **2017**, *65*, 1−14.

(19) Berguerand, N.; Lyngfelt, A. The Use of Petroleum Coke as Fuel in a 10 kWth Chemical-Looping Combustor. *Int. J. Greenh. Gas Control.* **2008**, *2*, 169−179.

(20) Markström, P.; Linderholm, C.; Lyngfelt, A. Chemical-looping combustion of solid fuels - Design and operation of a 100 kW unit with bituminous coal. *Int. J. Greenh. Gas Control.* **2013**, *15*, 150−162.

(21) Zevenhoven, M.; Yrjas, P.; Skrifvars, B.-J.; Hupa, M. Characterization of Ash-Forming Matter in Various Solid Fuels by Selective Leaching and Its Implications for Fluidized-Bed Combustion. *Energy Fuels* **2012**, *26* (10), 6366−6386.

(22) Sutton, D.; Kelleher, B.; Ross, J. R. H. Review of literature on catalysts for biomass gasification. *Fuel Process. Technol.* **2001**, *73* (3), 155−173.

(23) McKee, D. W. Mechanisms of the alkali metal catalysed gasification of carbon. *Fuel* **1983**, *62* (2), 170−175.

(24) Keller, M.; Leion, H.; Mattisson, T. Mechanisms of Solid Fuel Conversion by Chemical-Looping Combustion (CLC) using Manganese Ore: Catalytic Gasification by Potassium Compounds. *Energy Technol.* **2013**, *1* (4), 273−282.

(25) Mei, D.; Lyngfelt, A.; Leion, H.; Linderholm, C.; Mattisson, T. Oxygen carrier and alkali interaction in chemical looping combustion: case study using a braunite Mn ore and charcoal impregnated with K_2CO_3 or Na_2CO_3. *Energy Fuels* **2022**, *36*, 9470−9484.

(26) Bao, J.; Li, Z.; Cai, N. Promoting the Reduction Reactivity of Ilmenite by Introducing Foreign Ions in Chemical Looping Combustion. *Ind. Eng. Chem. Res.* **2013**, *52*, 6119−6128.

(27) Sevonius, C.; Yrjas, P.; Hupa, M. Defluidization of a quartz bed-Laboratory experiments with potassium salts. *Fuel* **2014**, *127*, 161−168.

(28) Zevenhoven, M.; Sevonius, C.; Salminen, P.; Lindberg, D.; Brink, A.; Yrjas, P.; Hupa, M. Defluidization of the oxygen carrier ilmenite−Laboratory experiments with potassium salts. *Energy* **2018**, *148*, 930−940.

(29) Gogolev, I.; Linderholm, C.; Gall, D.; Schmitz, M.; Mattisson, T.; Pettersson, J. B. C.; Lyngfelt, A. Chemical-looping combustion in a 100 kW unit using a mixture of synthetic and natural oxygen carriers − Operational results and fate of biomass fuel alkali. *Int. J. Greenh. Gas Control* **2019**, *88*, 371−382.

(30) Hildor, F.; Zevenhoven, M.; Brink, A.; Hupa, L.; Leion, H. Understanding the Interaction of Potassium salts with an Ilmenite Oxygen Carrier Under Dry and Wet Conditions. *ACS Omega* **2020**, *5*, 22966−22977.

(31) Gogolev, I.; Pikkarainen, T.; Kauppinen, J.; Linderholm, C.; Steenari, B.-M.; Lyngfelt, A. Investigation of biomass alkali release in a dual circulating fluidized bed chemical looping combustion system. *Fuel* **2021**, *297*, No. 120743.

(32) Gogolev, I.; Soleimanisalim, A. H.; Linderholm, C.; Lyngfelt, A. Commissioning, performance benchmarking, and investigation of alkali emissions in a 10 kWth solid fuel chemical looping combustion pilot. *Fuel* **2021**, *287*, No. 119530.

(33) Gogolev, I.; Pikkarainen, T.; Kauppinen, J.; Hurskainen, M.; Lyngfelt, A. Alkali emissions characterization in chemical looping combustion of wood, wood char, and straw fuels. *Fuel Process. Technol.* **2022**, *237*, No. 107447.

(34) Olsson, E. O. L.; Purnomo, V.; Glarborg, P.; Leion, H.; Dam-Johansen, K.; Wu, H. Thermal conversion of sodium Phytate using the oxygen carrier ilmenite interaction with Na-Phosphate and its effect on reactivity. *Energy Fuels* **2022**, *36*, 9423−9436.

(35) Andersson, V.; Stanicic, I.; Kong, X.; Leion, H.; Mattisson, T.; Pettersson, J. B. C. Alkali desorption from ilmenite oxygen carrier particles used in biomass combustion. *Fuel* **2024**, *359*, No. 130400.

(36) Purnomo, V.; Hildor, F.; Knutsson, P.; Leion, H. Interactions between potassium ashes and oxygen carriers based on natural and waste materials at different initial oxidation states. *Greenh. Gas Science Technolo.* **2023**, *13*, 520−534.

(37) Störner, F.; Knutsson, P.; Leion, H.; Mattisson, T.; Ryden, M. An improved method for feeding ash model compounds to a bubbling fluidized bed − CLC experiments with ilmenite, methane, and K_2CO_3. *Greenh. Gas Science Technolo.* **2023**, *13*, 546−564.

(38) Lu, D. Y.; Tan, Y.; Duchesne, M. A.; McCalden, D. Potassium capture by ilmenite ore as the bed material during fluidized bed conversion. *Fuel* **2023**, *335*, No. 127008.

(39) Hildor, F.; Yilmaz, D.; Leion, H. Interaction behavior of sand-diluted and mixed Fe-based oxygen carriers with potassium salts. *Fuel* **2023**, *339*, No. 127372.

(40) Leion, H.; Frick, V.; Hildor, F. Experimental Method and Setup for Laboratory Fluidized Bed Reactor Testing. *Energies* **2018**, *11*, 2505.

(41) Mei, D.; Soleimanisalim, A. H.; Lyngfelt, A.; Leion, H.; Linderholm, C.; Mattisson, T. Modelling of gas conversion with an analytical reactor model for biomass chemical looping combustion (bio-CLC) of solid fuels. *Chem. Eng. J.* **2022**, *433*, No. 133563.

(42) Cho, P.; Mattisson, T.; Lyngfelt, A. Defluidization conditions for a fluidized bed of iron oxide-, nickel oxide-, and Manganese oxide-containing oxygen carriers for chemical-looping combustion. *Ind. Eng. Chem. Res.* **2006**, *45*, 968−977.

(43) Purnomo, V.; Yilmaz, D.; Leion, H.; Mattisson, T. Study of defluidization of iron- and manganese-based oxygen carriers under highly reducing conditions in a lab-scale fluidized-bed batch reactor. *Fuel Process. Technol.* **2021**, *219*, No. 106874.

(44) International Organization for Standardization (ISO). *ISO 18134−2:2017. Solid Biofuels-Determination of Moisture Content-Oven Dry Method-Part 2: Total Moisture-Simplified Method*; ISO: Geneva, Switzerland, 2017.

(45) International Organization for Standardization (ISO). *ISO 18122:2015. Solid Biofuels-Determination of Ash Content*; ISO: Geneva, Switzerland, 2015.

(46) International Organization for Standardization (ISO). *ISO 18123:2015. Solid Biofuels-Determination of the Content of Volatile Matter*; ISO: Geneva, Switzerland, 2015.

(47) International Organization for Standardization (ISO). *ISO 16994:2016. Solid Biofuels-Determination of Total Content of Sulfur and Chlorine*; ISO: Geneva, Switzerland, 2016.

(48) International Organization for Standardization (ISO). *ISO 16948:2015. Solid Biofuels-Determination of Total Content of Carbon, Hydrogen and Nitrogen*; ISO: Geneva, Switzerland, 2015.

(49) International Organization for Standardization (ISO). *ISO 18125:2017. Solid Biofuels-Determination of Calorific Value*; ISO: Geneva, Switzerland, 2017.

(50) ASTM International. *ASTM D3682-13-Standard Test Method for Major and Minor Elements in Combustion Residues from Coal Utilization Processes*; ASTM International: West Conshohocken, PA, 2013.

(51) McKee, D. W. Gasification of graphite in carbon dioxide and water vapor-the catalytic effects of alkali metal salts. *Carbon* **1982**, *20*, 59−66.

(52) Śpiewak, K.; Czerski, G.; Porada, S. Effect of K,Na and Ca-based catalysts on the steam gasification reactions of coal. Part I: Type and amount of one-component catalysts. *Chem. Eng. Sci.* **2021**, *229*, No. 116024.

(53) Arjmand, M.; Leion, H.; Mattisson, T.; Lyngfelt, A. Investigation of different manganese ores as oxygen carriers in chemical-looping combustion (CLC) for solid fuels. *Applied Energy* **2014**, *113*, 1883−1894.

(54) Keller, M.; Leion, H.; Mattisson, T.; Lyngfelt, A. Gasification inhibition in chemical-looping combustion with solid fuels. *Combust. Flame* **2011**, *158*, 393−400.

(55) Mei, D.; Lyngfelt, A.; Leion, H.; Mattisson, T. Study of the interaction between a Mn ore and alkali chlorides in chemical looping combustion. *Fuel* **2023**, *344*, 9470−9484.

(56) Cheng, M.; Chen, S.; Zhu, H.; Zhao, X.; Bai, J. Promoting silicate formation by alkali chloride solid solution during thermal conversion of silicon-containing solid fuels. *Energy Fuels* **2024**, *38*, 6764−6773.

(57) Nakagawa, H.; Ono, Y. Effect of potassium chloride on the reduction of iron oxide. *Trans. Iron Steel Inst. Jpn.* **1985**, *25*, 1021−1024.

(58) Li, X.; He, F.; Su, X.; Behrendt, F.; Gao, Z.; Wang, H. Evaporation rate of potassium chloride in combustion of herbaceous biomass and its calculation. *Fuel* **2019**, *257*, No. 116021.

(59) He, Z.-M.; Cao, J.-P.; Zhao, X.-Y. Review of Biomass Agglomeration for Fluidized-Bed Gasification or Combustion Processes with a Focus on the Effect of Alkali Salts. *Energy Fuels* **2022**, *36*, 8925−8947.

(60) den Hoed, P.; Luckos, A. Oxidation and reduction of Iron-Titanium Oxide in chemical Looping Combustion: A Phase-Chemical Description. *Oil Gas Sci. Technol.* **2011**, *66* (2), 249−263.

(61) Corcoran, A.; Knutsson, P.; Lind, F.; Thunman, H. Mechanism for migration and layer growth of biomass ash on ilmenite used for oxygen carrier aided combustion. *Energy Fuels* **2018**, *32*, 8845−8856.

(62) Gogolev, I.; Soleimanisalim, A. H.; Mei, D.; Lyngfelt, A. Effects of temperature, operation mode, and steam concentration on the alkali release in chemical looping conversion of biomass- experimental investigation in a 10 kWth pilot. *Energy Fuels* **2022**, *36*, 9551−9570.